2018

# Principles of Surface Chemistry Central To the Reactivity of Organic Semiconductor Materials

Gregory J. Deye

LOYOLA UNIVERSITY CHICAGO

# PRINCIPLES OF SURFACE CHEMISTRY CENTRAL TO THE REACTIVITY OF ORGANIC SEMICONDUCTOR MATERIALS

A DISSERTATION SUBMITTED TO

THE FACULTY OF THE GRADUATE SCHOOL

IN CANDIDACY FOR THE DEGREE OF

DOCTOR OF PHILOSOPHY

PROGRAM IN CHEMISTRY

BY

GREGORY J. DEYE

CHICAGO, IL

AUGUST 2018

ACKNOWLEDGMENTS

The scientific advances and scholarly achievements presented in this dissertation are a direct result of excellent mentorships, collaborations, and relationships for which I am very grateful. I thank my advisor, Dr. Jacob W. Ciszek, for his professionalism in mentorship and scientific discourse. He took special care in helping me give more effective presentations and seek elegant solutions to problems. It has been a privilege to work at Loyola University Chicago under his direction. I would also like to express gratitude to my committee members, Dr. Wei-Tsung Lee, Dr. Daniel Killelea, and Dr. Jixin Chen who have aided me greatly by providing helpful and thought provoking feedback on my work. Dr. Jixin Chen was also an incredible collaborator with whom I had the pleasure of working. I am also very grateful to the Robert R. Otremba Scholarship and National Science Foundation for funding several years of my research at Loyola University Chicago.

My fellow colleagues and friends deserve a great deal of thanks: Juvinch R. Vicente, Bryan D. Paulsen, Selma Piranej, Demetra Adrahtas, Shawn M. Dalke, Dr. Brittni A. Qualizza, Dr. Dan Batzel, Hae Jun Park, Dr. Min He, and Dr. Paul Xu. I would also like to make special mention of Dr. Jonathan P. Hopwood whose friendship and collaboration played an important role during graduate school.

I wish to make a most sincere and loving thank you to my parents, Basia and Gregory D. Deye, for their support and for being incredible role models. I thank my brother, Robert

Komenda, for giving me unending motivation and levity. Lastly, I am extremely grateful for the exceptional role Dr. Stephanie M. Adib has played in my life these past six years.

To my loving parents,
Barbara and Gregory D. Deye

TABLE OF CONTENTS

LIST OF FIGURES

# CHAPTER ONE

# AN INTRODUCTION TO ORGANIC SEMICONDUCTOR SURFACES: THEIR PREVALENCE, STRUCTURE, AND REACTIVITY

Organic light emitting diodes (OLEDs),[1–5] organic photovoltaics (OPVs),[6–10] and organic field-effect transistors (OFETs)[11–15] are integral to modern electronic devices. The rise of these next generation devices can be credited, in part, to superior function and processing of the materials which comprise the device. Notable examples include solution processable organic semiconductor materials, which allowed for the utilization of cost-effective deposition methods including ink jet[16,17] or roll-to-roll printing.[18,19] The application of organic materials into electronics has also enabled bendable and wearable devices that are robust.[20–22] Generally, these low-cost, lightweight and flexible materials hold promise in supplanting existing more expensive conventional silicon-based electronics. In fact, the current market value for printed flexible organic electronics is $29.3 billion (USD) and is forecasted to grow to $73.4 billion by 2027.[23]

The materials utilized in organic electronic devices vary dramatically in structure and properties as dictated by the device function. All are highly conjugated small molecules or polymers (Figure 1, left). The extent of conjugation in the organic materials plays an important role in modulating the energies of the frontier orbitals. Organic materials with higher conjugation have lower energy LUMOs and higher energy HOMOs (e.g. the band gap of pentacene is ~1 eV lower than tetracene.)[24] Chemical functional groups bonded to organic materials modulate the energies of the frontier orbitals, and ultimately dictate the characteristic transport type. The

majority of organic molecules are electron rich p-type materials and have high energy LUMOs, and this makes hole transport through the HOMO more favorable. n-Type materials are electron deficient and often have π-accepting (cyano or carbonyl) or electron withdrawing (halogen) functional groups, which presents a lower LUMO that is easier to reduce. Of these, pentacene and tetracene will be utilized for the experiments herein as they are prototypical p-type materials for OFETs and OPVs.

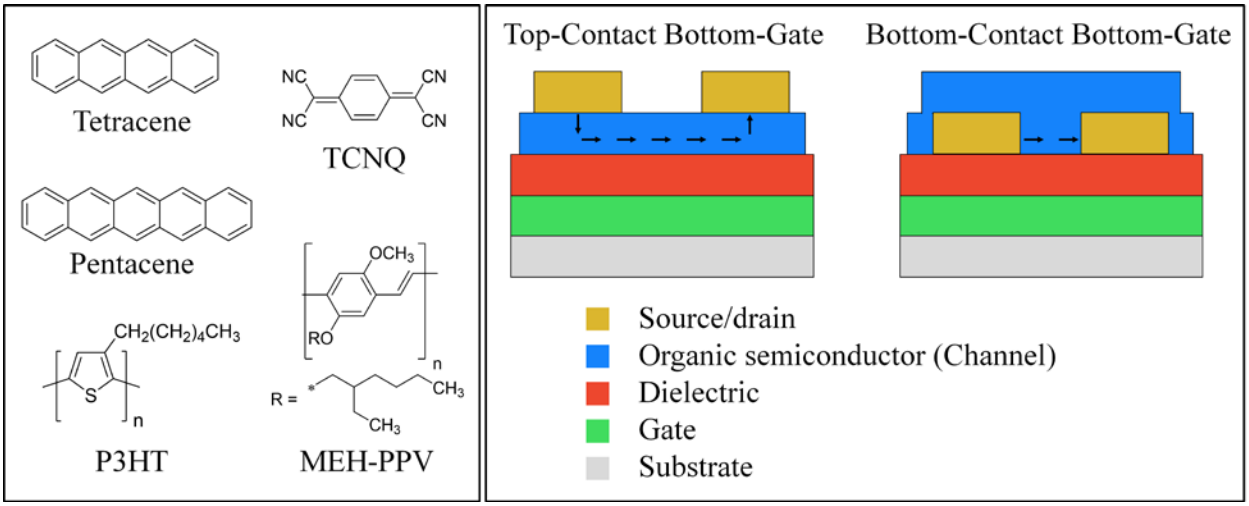


Figure 1. Left: Prototypical organic semiconductor molecules. Right: Two possible device architectures for OFETs. Arrows show the direction of charge carrier movement through the organic semiconductor channel.

Challenges arise with the incorporation of organic semiconductor molecules into devices and, if not addressed, they have the potential to undermine performance. In a typical device, such as an OFET, multiple layers of metal and organic films are deposited successively to form layered architectures (Figure 1, right). Each layer performs a specific function which contributes to device performance e.g. channels relay charge carriers from source to drain electrodes when in an “on” state. Of particular interest are the interfaces between them as they play a major role. When charge carriers are injected into the channel from the source/drain electrodes, they cross an organic-metal interface. As this occurs, the interface presents energetic barriers (to be discussed

shortly) that are either too high and limit injection, or low enough that energy loss is avoided. The interface is also where the strength of adhesion between the organic and metal layers is defined. Here, chemical functional groups on each surface determine the type of interactions (bonding or weaker noncovalent interactions), and an improperly designed interface results in delamination, or the peeling apart of the layers.[25–27] Not obvious from the illustrations is the fact that the quality of these interfaces is highly dependent on the *ordering of the layers* in the OFET, even if the same materials are used. In a bottom-contact bottom-gate arrangement, there are less processing challenges as the deposition of the organic semiconductor is the final processing step. Here, the underlying metal is robust, and simple surface modifications are possible. In contrast, for a top-contact bottom-gate arrangement, metal electrodes are patterned on top of the vulnerable organic semiconductor and often metal penetration or partial decomposition of the organic semiconductor[28–31] is an issue.

Interfaces between layers in a device are important, as this is where performance-impeding processes, such as charge injection barriers, arise if the surfaces are improperly engineered. In order for charge carriers to pass from between the metal electrodes and organic semiconductor, they must surmount an (Schottky) energy barrier. For a hole, (the dominant carrier in pentacene) this is the energy difference between the metal's Fermi level and the organic semiconductor's HOMO. Power is wasted when additional voltage must be supplied to surmount these barriers however, clever engineering of interfaces can eliminate this issue. For example, one way to manage the barrier is through inserting a monolayer, containing a sizeable dipole, on the metal.[32,33] The orientation of this dipole relative to the metal surface causes the metal's Fermi level to vary, and when oriented away from the surface, the Fermi level has been shown to decrease.

What the prior examples have in common is the improvement of the ***metal*** component of the electrode-organic semiconductor interface; interface modification useful for bottom-contact arrangements. In contrast, methods to improve the ***organic*** interface, which would be attractive in top-contact arrangements, remain largely unaddressed. Currently, only crude methods, such as photooxidation[34,35] and electron irradiation,[36] are used to chemically functionalize the surface, and they have poor reproducibility and depth control. The mechanism for these involves the production of highly reactive radicals which quickly react with the surface and into the subsurface. Another, milder, method is the polymerization of alkyl silanes off of oxygen defects on the organic surface.[37] Though this method tolerates a variety of chemical functional groups on the silanes, there are several inadequacies including reproducibility and poor coverage. Disappointingly, none of the methods take advantage of the inherent cycloaddition chemistry that π-bonds on organic semiconductor molecules are prone to. In contrast, the Diels-Alder reaction is an ideal candidate because each surface molecule possesses the chemistry necessary for reaction and there is a higher level of control.

On an organic semiconductor surface, the Diels-Alder reaction (Figure 2) occurs between π-electron rich dienes (organic semiconductor) and π-electron deficient dienophiles (adsorbates). Here, four π-electrons on the organic semiconductor and two π-electrons on the adsorbate concertedly rearrange to form two carbon-carbon bonds. For the reaction to occur, the adsorbate must position itself within 2.2 Å away from the organic semiconductor (transition state geometry).[38] A wide range of adsorbates, differing sterically and electronically, can be reacted with the surface. This is advantageous for the processing of organic semiconductors because having an arsenal of chemical functional groups to decorate the surface can significantly impact surface properties, including wettability. Indeed, a recent report, using contact angle

experiments, demonstrated a sizeable increase in the hydrophilicity of a tetracene thin film surface following exposure to maleic anhydride and *N*-hydroxymaleimide vapor (Contact angles of: tetracene (80°), tetracene reacted with maleic anhydride (66°), and tetracene reacted with *N*-hydroxymaleimide (60°).[39] While some initial success has been shown using Diels-Alder chemistry to functionalize organic semiconductor surfaces, including altering properties, the reaction of organic surfaces is very new and especially challenging.

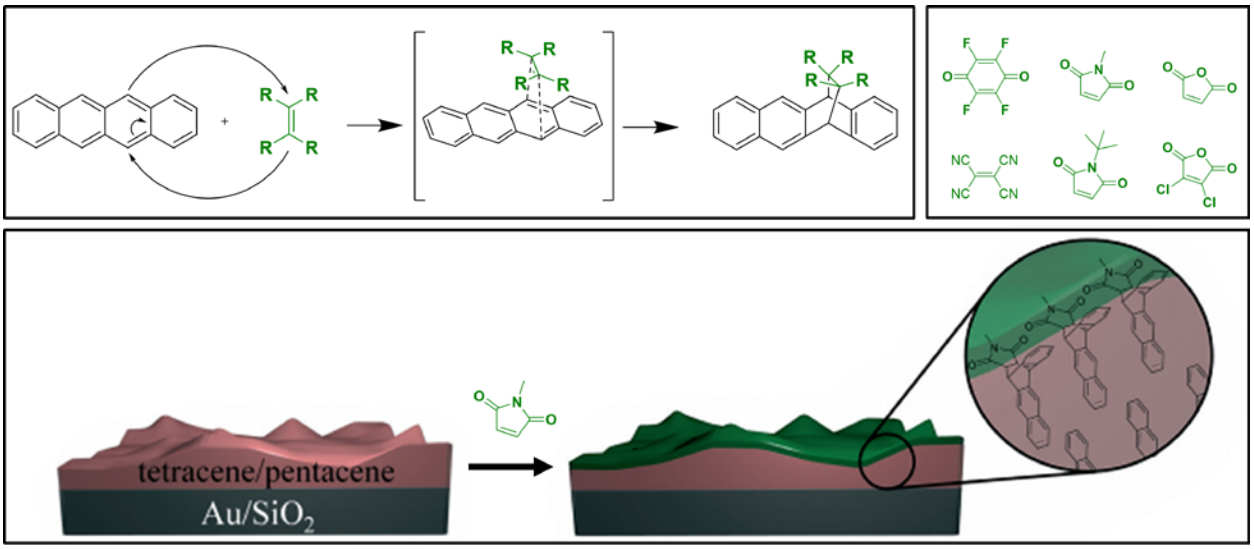


Figure 2. Top left: Diels-Alder reaction mechanism between tetracene (diene; black) and adsorbate (dienophile; green). Top right: Examples of adsorbates. Bottom: Tetracene/pentacene film surfaces undergo the Diels-Alder reaction with vapor phase *N*-methylmaleimide. Taken from reference 37 and reformatted.

## Challenges Presented by Surfaces

Broadly, surfaces have been an outstanding challenge in the scientific community for centuries, and even today. Professor Wolfgang Pauli, a renowned physicist, noted the complexity of the surface when he described it as being "invented by the devil."[40] Surfaces were referred to in this manner because of the massive disparities between surface and bulk atoms on a structural, energetic, and reactive basis. Structurally, bulk atoms are enveloped from all sides by stabilizing

metallic or covalent bonds, whereas surface atoms are not (Figure 3). The absence of overlaying bonding partners results in surface atoms having higher energy and more degrees of freedom. There is also the challenge of measuring low coverage implicit within surfaces. A single molecule thick monolayer would be equal to ~$10^{14}$ molecules/$cm^2$.[41] Assessing surface reactivity is also challenging because contaminants can readily occur at amounts far exceeding ~$10^{14}$/$cm^2$. In fact, contamination is so pervasive that ultrahigh vacuum and sputtered surface conditions are often required for analysis. These classical challenges in surface science also exist for organic surfaces, and in some cases, are exaggerated.

Organic surfaces are structurally different than their inorganic counterparts, conferring a new set of challenges associated with these surfaces. Namely, weak intermolecular interactions, anisotropic reactivity, and elaborative transition states play a sizeable role in reactivity. The weak van der Waals interactions between molecules in organic surfaces makes the surface susceptible to distortion and increased spacing; more so than with inorganic surfaces. As a result, it is feasible for adsorbed molecules on organic surfaces to diffuse into the subsurface and react with interior molecules. Next, there is a high degree of directional dependence associated with reactions on organic surfaces because, typically, only one site on a surface molecule is reactive. Therefore, the reaction rate is highly dependent on the orientation of surface molecules within the lattice (Figure 3). Reactions of organic surfaces are also challenging because of distinct transition state geometries. Since, adsorbates must position themselves at a particular distance and angle from the reactive surface molecule, this requires that adsorbates move and sample various geometries on the surface to chemisorb.

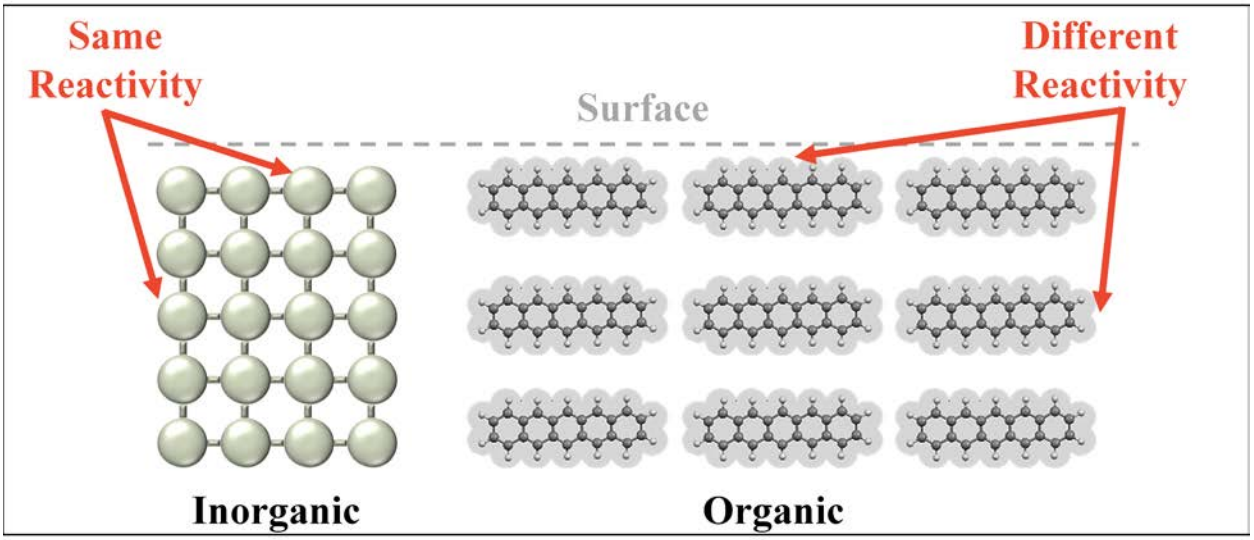


Figure 3. Differences between the surface and bulk are illustrated for inorganic (left; cubic lattice) and organic (right; pentacene) substrates. The red arrows highlight the importance of adsorbate approach to the two surfaces.

Fortunately, there is precedence for the reactivity of organic crystals in the form of solid phase reactions, and this may lend in predicting *surface* reactivity. In the 1970's, Paul and Curtin demonstrated *p*-chlorobenzoic anhydride crystals (and chemical derivatives) reacted when exposed to ammonia gas.[42,43] Despite only having crude methods for analysis, they were able to demonstrate the reaction occurred along axes, and through channels, of the crystal where reactive carbonyl functional groups were exposed. As chemisorption proceeded, ammonia propagated into the bulk of the crystal. Later, in the 1990's, Kaupp et al. performed solid-gas and dimerization experiments for the waste-free conversion of solids and reported the crystals reconstructed after exposure to reaction conditions. The formation of product molecules in the host lattice produced strain, and facilitated crystal transformation. Their examination also included (for the first time) surface characterization tools: atomic force microscopy (AFM) and near-field scanning optical microscopy (NSOM). While this work is influential in deducing bulk reactions of organic crystals, the reactivity of the surface remained unclear.

## Scope of Research on Organic Surfaces

In an effort to improve interfaces in organic electronics, a sound understanding of the guiding principles of reactivity of organic semiconductors is required. This dissertation seeks to address this by demonstrating guiding principles of reactivity as revealed during the exposure of acenes to Diels-Alder conditions. This is studied via the reaction of pentacene and tetracene which were chosen based on their prevalent use in organic electronics,[44] and precedence demonstrating their reactivity to cycloaddition chemistry.[39,45,46]

In chapter 2, the influence of the weak lattice on surface reactivity was examined, particularly with consideration of possible access to the subsurface. Because the organic surface is held together by relatively weak intermolecular interactions, modest temperatures may greatly affect the spacing between surface molecules. And as the work by Paul, Curtin, and Kaupp showed, temperature is likely to play an important role dictating adsorbates access to the subsurface. Next, the evaluation of classical reaction models were examined to assess the accuracy of the models in predicting surface reactions. To achieve this, two different reaction models, solid-state and solution, were evaluated against the Diels-Alder surface reaction. By systematically reacting pentacene and tetracene films with a host of adsorbates, and contrasting results to solution phase reactivity, results indicated reactivity of the organic surface was dependent on an amalgam of solution and solid-state factors.

Towards improving the organic surfaces in top-contact devices, this dissertation discusses the influence defects have on inducing reactivity of otherwise unreactive surfaces. Because it has been demonstrated on tetracene crystals that the (001) surface was unreactive to Diels-Alder chemistry, analogous pentacene (001) films with controlled defect density were prepared. Defect density on a nominally pentacene (001) thin film was manipulated using average grain size as a

means to vary the number of associated defects (vacancies and dislocations). Using thermally induced pentacene film growth, two disparate average grain sizes were obtained. Exposure of these films to vapor-surface Diels-Alder conditions resulted in reaction of the nominally (001) surface, and importantly, chemisorption correlated strongly with defect density. Further, the ability of adsorbates to propagate into the bulk crystal from defect sites was studied using tetracene crystals with only one or two surface defects. Analysis with scanning electron microscopy (SEM) revealed, indeed, the reaction initiated at a tetracene dislocation, and propagated several microns from the higher terrace.

The work presented in this dissertation was well-received through various scientific communities. At the Materials Research Society Spring Meeting, materials scientists and engineers were eager to learn that the Diels-Alder reaction showed promising results in improving the organic surface component of the metal/organic interface in organic electronics. Meanwhile, the surface science community at the AVS Prairie Chapter valued hearing about the reactivity of organic semiconductor surfaces. The work from chapter 2 was published in Langmuir[47] and Chapter 3 is in preparation for publication. In time, I anticipate the Diels-Alder reaction of organic semiconductor surfaces will prove valuable to improve interfaces in organic electronics.

In the future, for the Diels-Alder surface reaction to realize application in the commercial processing of organic electronics, I foresee two checkpoints that need addressing. The first is the application of this chemistry to a broader class of organic semiconductors, such as soluble organic semiconductors and polymers. A broad class of organic semiconductor surfaces will validate the near ubiquitous application of the Diels-Alder reaction. Next, it would be useful to demonstrate the versatility of the processes to apply Diels-Alder chemistry to surfaces. More

specifically, developing a method to selectively pattern reacted areas would allow for more sophisticated organic electronic designs.

CHAPTER TWO

# THE ROLE OF THERMAL ACTIVATION AND MOLECULAR STRUCTURE ON THE REACTION OF MOLECULAR SURFACES

## Introduction

The surface chemistry of molecular substrates has recently garnered much attention,[39,48,49] driven by the need to optimize interfaces in organic optoelectronic devices.[14,50–54] Several rudimentary methods of chemical functionalization have been demonstrated, such as UV-ozone treatment,[34,35] where a layer of oxidized molecules are generated at an organic surface and eventually randomly propagated into the subsurface; and homolytic bond reorganization induced by electron irradiation.[36] However, the ideal embodiment of surface functionalization would be flexible, well-defined, and contain chemistry specific to these new substrates. This was first hinted at by Calhoun et al. who showed that it is possible to polymerize alkyl silanes off of oxygen defects on rubrene, in a manner reminiscent of silicon oxide/silane chemistry.[37] Though more versatile, defect directed reactions have poor repeatability, as defect coverage is poorly defined, and they leave a majority of surface molecules untouched. The obvious next step was to take advantage of the inherent surface reactivity of each of the molecules on the organic surface. In doing so, adsorbate molecules could be appended one per surface molecule and generate robust and well-defined surface structures.

Recently, a surface modification approach which fulfills these requirements has been demonstrated. We have published work on the reaction of acene surfaces (linearly fused benzene rings), whereby traditional solution chemistry has been used as a template for surface-based reactions.[39,45,46] The acene substrates were particularly appealing as they contain electron rich π-systems, and are primed for classical Diels-Alder cycloaddition chemistry.[55] In the solution phase, this chemistry has been applied to anthracene prolifically (thousands of publications available in the literature), providing ample guidance for this approach. Additional advantages include modest reaction conditions, no side-products, and the compatibility with various functional groups. We have demonstrated that a host of molecular adsorbates can be reacted at the interface of these organic substrates using Diels-Alder cycloaddition chemistry (Figure 4).[39] Acene thin films that are exposed to volatile dienophiles react, one per surface molecule, forming the same species as is produced via traditional solution chemistry.[46] This application of classical synthetic chemistry to organic surfaces appears a powerful addition to the needs of materials scientist and has the potential to usher in a new chapter in surface chemistry.

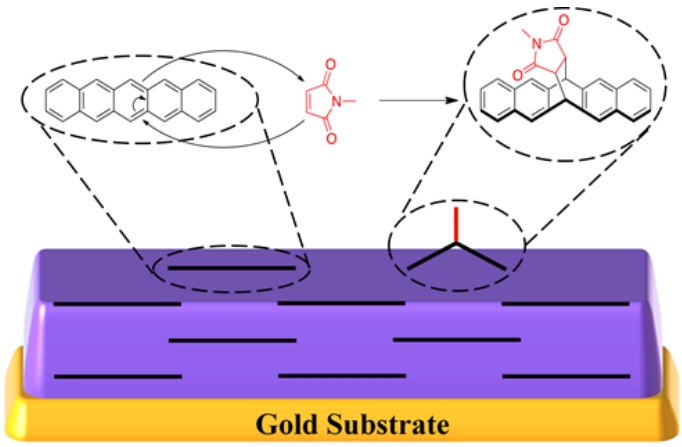


Figure 4. General mechanism for the Diels-Alder reaction between gas phase *N*-methylmaleimide and a pentacene thin film. Curved arrows indicate the direction of electron movement during covalent bond formation.

The challenge here is that the field of organic surface chemistry is in its infancy, and as such, there is little precedence for modeling surface reaction behavior. It is inadequate to directly compare the reactions on organic thin films to the reactions on traditional inorganic surfaces. Acene molecules within the lattice interact exclusively through weaker noncovalent molecular interactions (van der Waals, π-interactions) and the intermolecular spacing is quite large (Figure 5). In comparison, inorganic counterparts have strong metallic or covalent bonds between atoms, and spacing between atoms is below van der Waals distances.[56] These differences bring two new features to the surface reactions on organic thin films. First, the non-covalent makeup of the lattice means significant voids exists within the solid, and channels are common. These channels present a pathway for larger adsorbates (>3 Å) to diffuse into the solid, one that does not exist in inorganic substrates. For example, crystalline thiohydantoins and carboxylic acid derivatives have been completely consumed during their reaction with gaseous alkyl amines, facilitated by small channels within the lattice. [42,57,58] This subsurface accessibility contrasts with traditional inorganic surfaces, where subsurface reactivity is confined to mono/di/tri-atomic adsorbates.[59,60] Second, the weak interactions mean the lattice is susceptible to significant deformation at or near room temperature, resulting in another mechanism for the organic vapors to diffuse into the solid. For example, vinyl bromide readily diffuses into calixarene crystals at -5 ºC despite the structure lacking channels.[61] Both features suggest that the occurrence of subsurface and bulk reaction might be common in organic solids, and should be examined when developing surface functionalization methodologies.

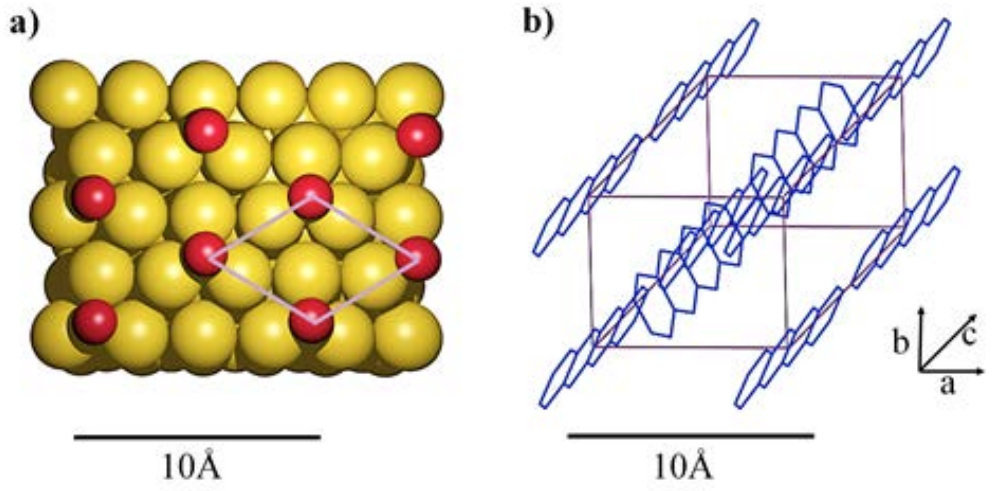


Figure 5. Differences in lattice spacing for inorganic and organic substrates are illustrated. Figure scales are consistent to allow comparison. (a) Au(111) with a thiol monolayer on top adopts a $(\sqrt{3}\times\sqrt{3})R30^{o}$ structure. Red spheres (sulfur) are drawn in a hollow site position for visual simplicity since the chemical bonding motif is dramatically more complex.[62] (b) Unit cell of tetracene.[63]

Because of the potential for adsorbates to readily diffuse into the subsurface, we have reexamined the reaction of vapor dosed dienophiles onto acene thin films. Herein, we demonstrate that the subsurface and bulk of acene thin films are accessible to a Diels-Alder reaction if the reaction is thermally activated. In the case of extensive reaction, topological changes occur; these are assessed and correlated to the chemical changes in the film. This methodology is then extended to various adsorbates/acene combinations, and the trends in kinetics allow us to assess whether diffusivity outweighs the influence of chemical activation barriers, in terms of determining reactivity.

## Experimental Section

### Materials

All metals used for evaporation were of 99.9% or greater purity. Sublimed grade pentacene and tetracene were commercially obtained and used without further purification.

Adsorbate source material used in the reaction of acene films (*N*-methylmaleimide, maleic anhydride, maleimide, *N*-methylsuccinimide, and tetrafluorobenzoquinone) were also commercially obtained and are of 97% or greater purity. ACS grade chloroform was used for solution phase kinetic studies.

**Preparation of Acene Thin Films**

Microscope slides (11 × 25 × 1 mm) were piranha cleaned (3:1 $H_2SO_4$: $H_2O_2$), rinsed twice with 18 MΩ deionized water and sonicated for 20 min. The substrates were rinsed with copious amounts of 200 proof ethanol before drying under a stream of nitrogen. Substrates were placed in a Kurt J. Lesker NANO38 thermal evaporator for metal deposition. At a base pressure of $5.0 \times 10^{-7}$ Torr, a chromium adhesion layer (5 nm) was deposited, followed by 50 nm of silver, and 50 nm of gold (all at 1 Å/s). Immediately following metal evaporation, the organic semiconductor was deposited using a home built sublimation chamber with a source to sample distance of 16–17.5 cm. 60 nm of acene were sublimed onto the metal-coated substrates at a base pressure of $<5.5 \times 10^{-6}$ Torr at a rate of 1 Å/s. Film thickness was monitored using an Inficon SQM-160 quartz crystal microbalance.

**Solid-State Diels-Alder Reactions**

Acene thin-film substrates were placed into a 100 mL Schlenk tube sealed with a hollow end stopper along with approximately 8 mg of solid adsorbate in a small vial. The air within the Schlenk tube was evacuated and replaced with nitrogen three times, and the sealed vessel was then heated in a furnace at the temperatures described in the text. After the reaction (18-24 h), the vapor phase dienophiles were condensed away from the substrate by cooling one end of the flask with dry ice. Any physisorbed material was removed by first exposing the sample to $< 10^{-2}$ Torr (roughing pump) for 15 min before subjecting it to pressures $< 10^{-5}$ (turbomolecular pump)

for 1 h.

**Infrared Analysis of Thin Films**

Composition of thin films were assessed both before and after reaction via PM-IRRAS using a Bruker Optics Tensor 37 FTIR equipped with a PMA 50 accessory and MCT detector. Reaction progress was assessed by comparing newly generated infrared vibrations to those within a spectrum of a standard solution synthesized adduct.[39] Additional information was gleaned from the consumption of substrate peaks. Thin films were analyzed at resolution of 8 $cm^{-1}$.

**AFM Analysis of Thin Films**

Surface morphologies of the pristine and reacted films were analyzed using atomic force microscopy (AFM) (MFP 3D microscope, Asylum Research) in tapping (non-contact) mode using a diamond-like-carbon coated AFM tip (Tap190DLC, Budget Sensors). The root-mean-square (rms) roughness of the film was calculated by the AFM software. In order to measure the film thickness, a small area of the film was removed by nanoshaving using the same tip under contact mode (force set point 0.5 V). The tip spring constant is ~40 N/m (with an estimated force of ~ 2 μN/V), meaning ~1 μN was applied to remove the organic film. At the end of the shaving, the gold surface was exposed at the bottom of the well. The force applied during the nanoshaving was confirmed to have no scratching effect on a bare gold surface. Then the AFM was switched back to tapping mode to image a larger area at the same location. The film thickness was calculated as the average depth of the well using the statistical tool of the AFM software.

**UV-vis Kinetics Measurements (Solution Reference Experiment)**

Rate constants for the reactions of pentacene with adsorbates *N*-methylmaleimide, maleic

anhydride, maleimide, and tetrafluorobenzoquinone (pseudo-first order) were obtained for the *solution* Diels-Alder reactions by monitoring pentacene consumption as a function of time via UV-vis (Shimadzu UV-2550), in a manner described previously.[45] Briefly, the pentacene ($2.6 \times 10^{-4}$ mM) was reacted under pseudo-first order conditions with a large excess of dienophile ($4.4 \times 10^{-2}$ mM, the adsorbate in analogous thin-film experiments). The reactions occurred at room temperature (20-25 °C) in degassed chloroform. The pentacene consumption was monitored via absorbance at the lowest energy excitation at 576 nm. In all experiments, the background absorption from the large excess of dienophile is subtracted out from spectra. In the case of tetrafluorobenzoquinone this was especially significant.

## Results and Discussion

The only forces between organic molecules within molecular substrates are noncovalent interactions. As a consequence, molecular solids have low lattice energies, on the order of 30 kcal/mol for the molecules herein,[64–67] making the surface susceptible to distortion. In addition, the intermolecular spacing in the organic thin film is relatively large comparing to the size of the adsorbates. Thus, we hypothesize that sub-surface reactions may become significant in these organic thin films. While this structure-driven subsurface reaction behavior was not originally recognized in our initial studies (at 50 ºC),[39] this work examines different temperature regimes in order to demonstrate a subsurface reaction. To test this hypothesis, ~60 nm-thick uniform pentacene thin films were exposed to and reacted with vapor phase *N*-methylmaleimide at elevated temperatures. The reaction kinetics and the change of the thin-film morphology is measured to study how dosed molecules can react beyond the surface into the subsurface. *N*-methylmaleimide was chosen as an adsorbate because of previously demonstrated surface reactivity and because the van der Waals dimensions of the molecule (7.5 Å at its largest

point)[68] are representative of most potential adsorbates for this reaction. Experiments began with an initial temperature range of 30 - 75 ºC, a range where lattice deformation might become significant.

The thin films, before and after reactions, were characterized with polarization modulation infrared reflection absorption spectroscopy (PM-IRRAS) to provide a quantitative measure of both the remaining subsurface pentacene and the extent of surface reaction. Specifically, pristine pentacene is observed via intense out-of-plane vibrations near 910 and 730 $cm^{-1}$, both of which occur in regions with no interfering bands from the reacted species.[45,69] As adsorbate molecules chemisorb to the pentacene thin film, the intensity of these infrared bands diminishes, which is presumed (and later confirmed) to come primarily from reaction, not volatilization/sublimation. Chemisorption is also observed via the growth of vibrations at 1776, 1700, 1280 and 1260 $cm^{-1}$.[39]

From the *N*-methylmaleimide reaction with pentacene thin films at 30, 50, and 75 ºC for 24 h, it is evident that a small change in temperature plays an outsized role, as the three substrates now have a dramatically different composition (Figure 6). Using the 910 $cm^{-1}$ vibration to measure the amount of retained pentacene, it is clear that at 30 ºC (blue) little change has occurred within the pentacene; when compared to the unreacted substrate (black line), virtually no change in the intensity of the vibration is observed. This is in contrast to the ~29% decrease at 50 ºC, and in strong contrast to the complete consumption of pentacene at 75 ºC. Thus, with minimal temperature increase, the pentacene thin film is consumed entirely. Complimentary data, acquired by monitoring adduct formation, provides a more detailed picture. At 30 ºC, adduct formation is confirmed via a growth in the four aforementioned standard product peaks (1776, 1700, 1280 and 1260 $cm^{-1}$). Consistent with the small decrease in

pentacene absorption, the amount of product generated is small. In fact, if an unmodulated IRRAS experiment is performed (Figure S1), the 1700 $cm^{-1}$ stretch appears to be of an intensity appropriate for a monolayer worth of material.[70] Throughout the rest of the temperature range, there appears to be equipoise consumption of substrate and production of product as apparent in Figure 3.

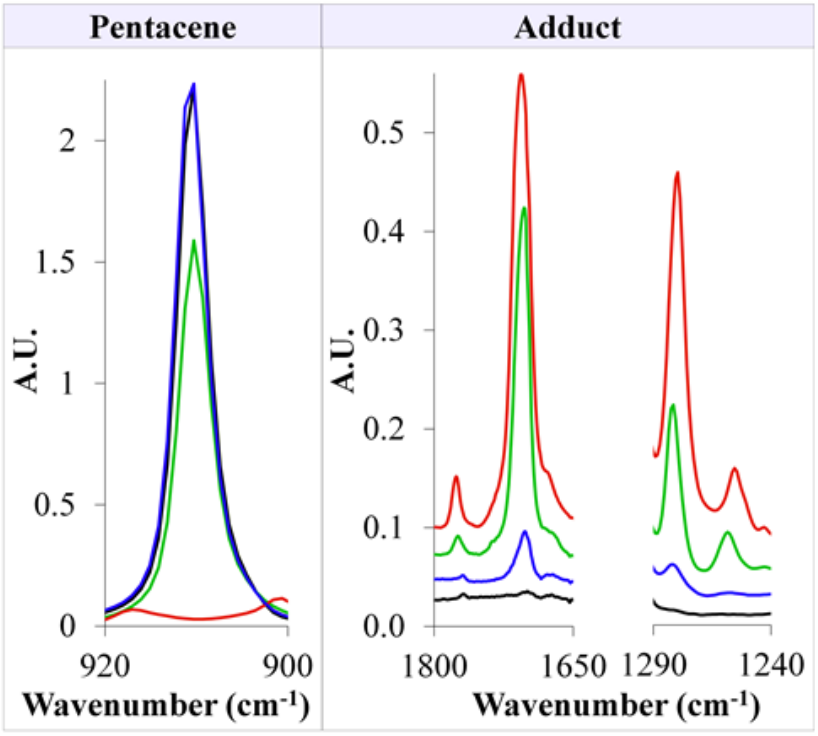


Figure 6. PM-IRRAS spectra of the multi-temperature (30, 50, 75 °C), 24 h reaction between pentacene and *N*-methylmaleimide. The color scheme is as follows: black (pristine pentacene), blue (30 °C), green (50 °C), and red (75 °C). Adduct vibrational modes have been offset for visual clarity.

Besides adduct formation, there are two other possible reasons for the diminished infrared pentacene bands: volatilization and thin-film annealing.[71] To quantify these effects, a pristine pentacene film from the same batch was heated at 75 °C for 24 h in the absence of *N*-methylmaleimide. All infrared peaks pertinent to pentacene decreased in intensity by an average of 13%, suggesting volatilization of a small fraction of the material (Figure 7 and S2). This

experiment also allows us to conclude that annealing of the thin film appears unlikely; if annealing caused the vibration at 910 $cm^{-1}$ to decrease, the infrared bands at 1445 and 1162 $cm^{-1}$ would have increased as molecules reorient relative to the surface normal.[39,69]

To further quantify pentacene volatilization, AFM was used to measure the thickness of the film. Because organic thin films are softer than inorganic substrates, an AFM tip in contact-mode can displace material and scratch through the pentacene down to the underlying gold support substrate, while the same force is not enough to scratch the bare gold surface. Subsequent line scans across the scratched area provide information regarding film thickness.[72] Scratched pentacene films that had been heated to 75 °C were found to have 9 nm less material than a sample maintained at 25 °C (61 nm). This 15% decrease is nearly identical to our IR analysis. The results also indicate that thin-film volatilization is non-negligible at 75 °C, but chemisorption is the dominant mechanism responsible for complete consumption of pentacene signal at 910 $cm^{-1}$.

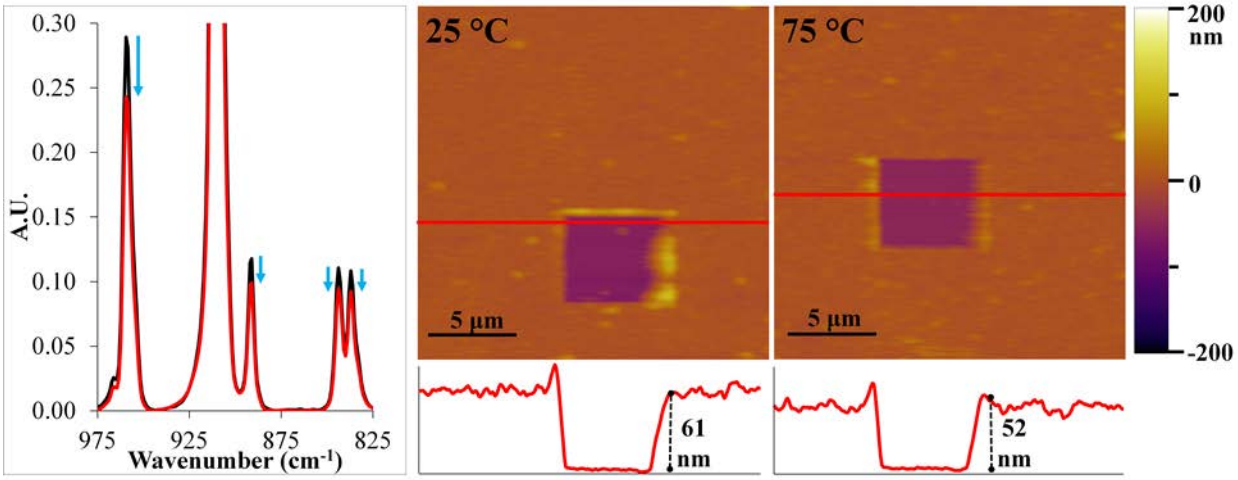


Figure 7. (left) PM-IRRAS and (right) AFM measurements of a pentacene substrate heated to 75 °C for 24 h allow for quantification of substrate volatilization. Both the absorption difference (13% average) and thickness change (9 nm, 15% difference) measure similar amounts of pentacene loss.

When considering the fact that the pentacene substrate reacted with *N*-methylmaleimide at 75 °C has been completely converted to adduct, it seems obvious to ask whether this surface maintains a filmlike arrangement because the reactants and the products have significantly different shape, packing, and crystal structures. When the substrates are examined by AFM, the answer is unambiguously no. AFM reveals the presence of irregular and dendritic structures on the surface (Figure 8, far left) with heights several hundreds of nanometers in size. It is natural to question how these features arise, and when surface integrity is lost. Thus, lower temperature samples were reexamined to observe the progression of the surface topology. The surface features, whether a form of increased roughness or localized reacted material, appear in all samples, but their form changes, and they appear less as the reaction temperature decreases. Features are still significant at 50 ºC and appear more as simple protrusions; by 30 ºC, coverage is sparse and heights are modest (Figure 8, middle two images). Samples at additional temperatures (25, 35, 40, 65 ºC) provide clarification of how the surface topology evolves. The rms of the substrates starts near that of pristine pentacene for a 25 ºC reaction, then exponentially increases at temperatures up to 35 °C, whereby the increase slows, and levels after a reaction temperature of about 40 ºC (Figure 8 right and Figure S3). After remaining constant from 40-65 ºC, the rms increases dramatically upon a small temperature increase to 75 ºC as the surface completely reorganizes. As rms data in Figure 8 shows, the surface morphology develops in three distinct regions, the largest of which (40-65 ºC) has significant surface protrusions with little variance in size and coverage over a span of 25 °C. The protrusion size mirrors RMS data (Figure S4).

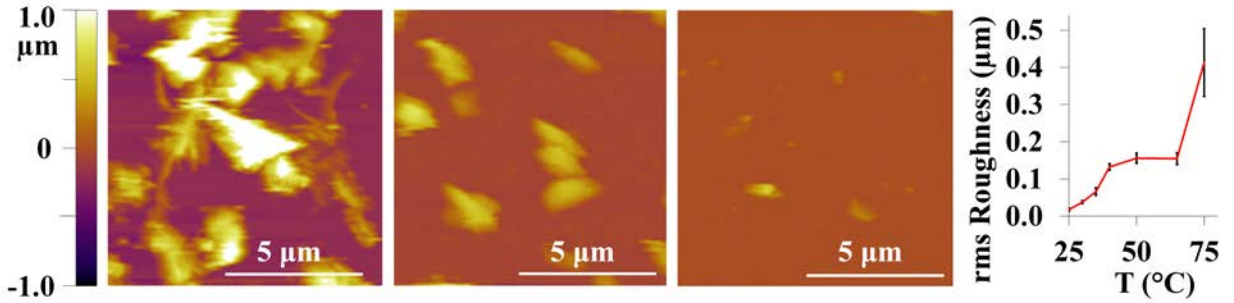


Figure 8. Left: AFM images of 75, 50, and 30 °C pentacene thin films reacted for 24 h with *N*-methylmaleimide. Right: Plot of average rms roughness values of reacted substrates helps quantitatively differentiate the three distinct regimes (near-pristine, protrusion covered, and complete film reorganization). Error bars of the standard deviation are included (see Table S1 for rms values). RMS data includes protrusions; data for the region between protrusions are found in Figure S5.

We have further investigated the 50 ºC sample to confirm that the surface protrusions at this temperature were on top of the contiguous pentacene layer rather than islands of pentacene separated by bare gold. Similar to the scratching experiments above, the 50 ºC sample was scratched with the AFM tip to identify the presence of an underlying organic layer, and to determine its thickness. The data demonstrate the underlying pentacene surface is still a continuous film after the reaction at this temperature (Figure S4), as a 40 nm thick film still exists in between the protrusions. The decrease of the thickness also suggests that surface migration of product is the likelier mechanism behind protrusion formation; that is, the surface layer of pentacene reacts with *N*-methylmaleimide, and the products segregate into the clusters on top of the pentacene layer.

Taken together, the temperature data suggest three distinct regimes for the reaction of pentacene thin films: *up to 30 ºC*, the reaction is on the order of a monolayer with little change to the thin film; *from 40 to 65 ºC*, the reaction progress extends further into the surface, and significant protrusions are now seen, but the unreacted pentacene maintains its original film

structure; *by 75 ºC* film structure has been destroyed. There are two other features of the data that are worth highlighting. First, the size of the *N*-methylmaleimide (7.5 Å) adsorbates are quite large, and the accessibility to the subsurface material (regardless of mechanism) is noteworthy. Second, the presence of the three distinct surface reaction regimes is remarkable for the fact that a pristine surface is completely restructured over a 50 °C temperature range. The extent of change these acene thin films undergo demonstrates the susceptibility of organic substrates to thermal influence, and is potentially due to weak forces between molecules; hence, attention is next focused on how much intermolecular forces influence reactivity and if they have any predictive use.

At first glance, the strength of the intermolecular forces among the thin-film molecules should determine the thin-film's subsurface reactivity. The pentacene lattice does not have an channel to allow for adsorbate penetration, and thus dynamic reorganization of this lattice[61] is the only way that adsorbates can diffuse within the solid. Lattice energy would track with the ability of the surface to reorganize, making it likely that substrates with weaker interaction (e.g. tetracene) display higher rates of subsurface reaction. This model does, however, make the over assumption that the reaction is in a regime where diffusion to the subsurface limits reactivity. Alternatively, the slowest step could be the ability of the adsorbate to reach a sterically appropriate transition state structure and by chemical activation barriers to bond formation. Here, the reaction may display trends in rates similar to classical solution chemistry. This would be especially fortuitous since there have been minimal computational studies on reactions of organic surfaces, but extensive studies in the solution phase.[73] Phrased another way, does the acene film's reactivity resemble molecular behavior or are they dictated by solid state properties.

On the basis of the above results of reacted pentacene thin films, it is difficult to assess

if lattice energy or chemical activation barriers are a primary driving factor for reactivity. In order to examine the degree each factor influences reaction behavior, we compared reactivity of organic substrates that have different lattice energies. Two different acenes (tetracene and pentacene) are chosen for this experiment because they have significantly different lattice energies of -32.0 kcal/mol[66] and -39.5 kcal/mol,[67] but have similar structure and a similar packing motif. Pentacene and tetracene thin films were reacted under the same Diels-Alder conditions described above (18 h reaction with gas phase *N*-methylmaleimide at 50 °C) for these experiments. Within the reacted substrates, the carbonyl stretch was used as a primary measure of reaction because of its large intensity and consistency in structure. In the diffusion-limited regime, both films should react significantly slower the solution reaction rate while at the same time the substrate with lower lattice energy is impacted less than the higher energy one.

Counter to expectations, the reaction of tetracene demonstrates that chemical activation barriers are the more significant contributor to subsurface reactivity in thin films. It is generally accepted that the chemical activation barrier is lower for pentacene because its electron rich central ring makes for more favorable diene-dienophile interactions.[74] In the solution phase, UV-vis kinetic experiments revealed *N*-methylmaleimide reacts 7 times faster with pentacene compared to tetracene.[45] Similarly, thin film of pentacene reacts faster than tetracene. Here the rate for pentacene is 1.7 times faster, as measured by the product's carbonyl stretch (Figure 9). Any lattice effects appear limited to the smaller difference between rates in the solid state. The result suggest that chemical activation barriers should be strongly considered, and the next question is whether this is general to other adsorbate combinations, or specific to these pairings.

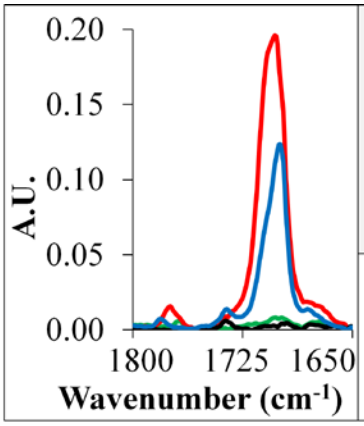


**Reaction with *N*-methylmaleimide**

| A.U. ($\nu_{CO}$) | Surface | Solution Relative Rate(k)[15] |
|---|---|---|
| 0.20 | Pentacene | 7 |
| 0.12 | Tetracene | 1 |

Figure 9. The carbonyl vibration for the reaction between pentacene and tetracene thin films with *N*-methylmaleimide at 50 °C for 18 h. Color scheme: pristine pentacene (black), reacted pentacene (red), pristine tetracene (green), reacted tetracene (blue). Within the table, solid state and solution phase reactivity are compared for tetracene and pentacene substrates.

To probe the importance of chemical activation barriers on reactivity, further thin-film experiments were performed. Here, pentacene was dosed with a series of adsorbates (tetrafluorobenzoquinone, *N*-methylmaleimide, maleimide, and maleic anhydride) known to have similar steric demands and comparable vapor pressures,[75] but different reaction rates in solution (Figure 10, S5). This approach eliminates the variability between substrates and thus provides more precise rate data. Reaction progress in the solid state (50 °C, 18 h) was determined by monitoring consumption of the pentacene film at 910 $cm^{-1}$. Any similarity between the trends in reaction rate between solid state and solution would further support the premise that chemical activation barriers can, to a first approximation, predict thin-film reactivity.

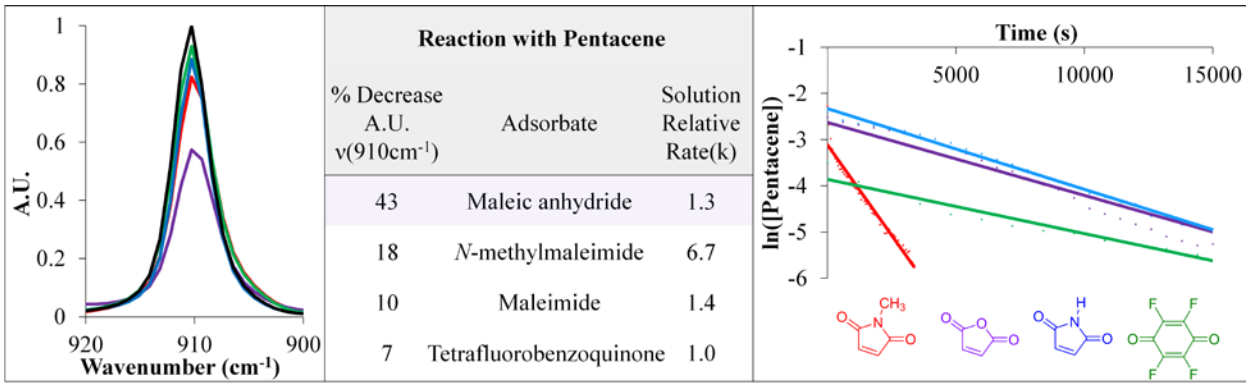


Figure 10. Comparison of thin film (left) and solution phase (right) pentacene kinetic trends. The PM-IRRAS spectra of multiple thin films were normalized and averaged (see Figure S6 and accompanying supporting information for details and complete spectra). The color scheme is as follows: unreacted pentacene (black), tetrafluorobenzoquinone reaction (green), *N*-methylmaleimide reaction (red), maleic anhydride reaction (purple), maleimide reaction (blue).

By ignoring the maleic anhydride data for a moment, the rest of the data are consistent with the prior conclusion that reaction energy barriers are highly correlated to the thin-film reactivity. The reactivity trend of the remaining three adsorbates in solution is *N*-methylmaleimide > maleimide ~ tetrafluorobenzoquinone while the reactivity trend for the pentacene thin films is *N*-methylmaleimide > maleimide > tetrafluorobenzoquinone (Figure 10). Thus both phases have an identical activity series for the adsorbates. Within this broader conclusion, there is also reoccurring evidence that the solid structure plays a role measurable role. Similar to the previous experiment, reactivity differences are dampened in the solid state. For example, *N*-methylmaleimide reacts 2.6 times faster than tetrafluorobenzoquinone on pentacene thin films and 6.7 times in solution. This difference in ratio indicates that the size and shape of the reactant, and the interaction between the thin film and the reactant contribute to the subsurface reactivity.

There appears to be one exception to this trend: maleic anhydride (although this molecule is also the least reliable among the four with the largest standard deviation). We

speculate that the larger variation (and potentially its difference in activity) is because the reaction temperature is close to maleic anhydride's melting temperature (52.8 °C)[76] but far from the others (all exceeding 94 °C). Thus, small variations in temperature have outsized impacts on the phase of maleic anhydride. Nevertheless, the results show maleic anhydride has moderate reactivity in solution while it is was the most active in the thin film.

It is also worth highlighting the relationship between maleimide and *N*-methylmaleimide. In solution, *N*-methylmaleimide reacts faster than the unsubstituted maleimide with pentacene. This also occurs in the thin films (Figure 10), which noteworthy as the *N*-methylmaleimide contains an additional methyl group which contributes steric hindrance to the reaction. While this does not impact solvated molecules appreciably, it was surprising that there were minimal effects at the surface. The consistent trend in reactivities between solution and thin films lends further support to the hypothesis that adsorbate diffusion in the thin film plays a more limited role in the reaction kinetics. This is a bit of a surprise as packing and steric effects were quite pronounced on the surface Diels-Alder reactions of tetracene single *crystals*.[46] With the wide range of substituents that can be appended to the adsorbates, this represents an interesting avenue to pursue.

## Conclusions

The reactivity of molecular substrates was evaluated by performing the Diels-Alder reaction on acene thin films. Structural features of this class of materials such as intermolecular spacing and weak noncovalent molecular interactions were instrumental in the ability of gaseous adsorbate molecules to react at both surface and into the subsurface of the substrates. PM-IRRAS revealed elevated reaction temperatures exaggerate this effect; complete reaction of the pentacene substrate (with *N*-methylmaleimide) occurred at a temperature only 45 °C higher than

monolayer coverage. Reaction into the subsurface also caused considerable morphology changes on the surface, as shown by AFM. Reactions of pentacene and tetracene films revealed lattice energy did not limit reactivity appreciably. Rather, the systems behaved as they do in the solution phase with chemical activation barriers appearing to be the primary determinant of reactivity, though some exceptions (maleic anhydride) shows empirical precedence from solution is not always a perfect predictor for describing reactivity of molecular substrates. The results ultimately demonstrate molecular substrates react like an amalgam of solid-state and solution factors.

CHAPTER THREE

# THE INFLUENCE OF DEFECTS ON THE REACTIVITY OF ORGANIC SURFACES

## Introduction

Before organic films are adopted into optoelectronic devices, interfacial flaws like poor adhesion and charge injection barriers must first be addressed.[32,39,47,77–79] Of the available methods to improve the organic surface, the Diels-Alder reaction is an elegant solution because the π-electron rich molecules are primed for chemistry with electron deficient adsorbates. This reaction has been demonstrated with the prototypical semiconductor pentacene,[39,47] however, molecular orientation within the film limits the range and applicability of the reaction. Here, the ideal orientation for pentacene is a facedown configuration on the substrate where the reactive □-system is exposed to approaching adsorbates (Figure 11, left). The most common (and less ideal) configuration is where molecules orient ~68° from the surface in the thin-film phase.[69] In this orientation, the predominant crystal face exposed is the (001) face and, at the surface, only unreactive C-H bonds are presented to the adsorbates (Figure 11, right). In fact, when this is transposed to the unblemished surfaces of single crystals, the (001) facets have been demonstrated to be inert to Diels-Alder reaction conditions.[46] This bodes poorly for thin-film phase pentacene as the (001) surface forms the majority of the interface with deposited metals in top-contact organic thin-film transistors (OTFTs).

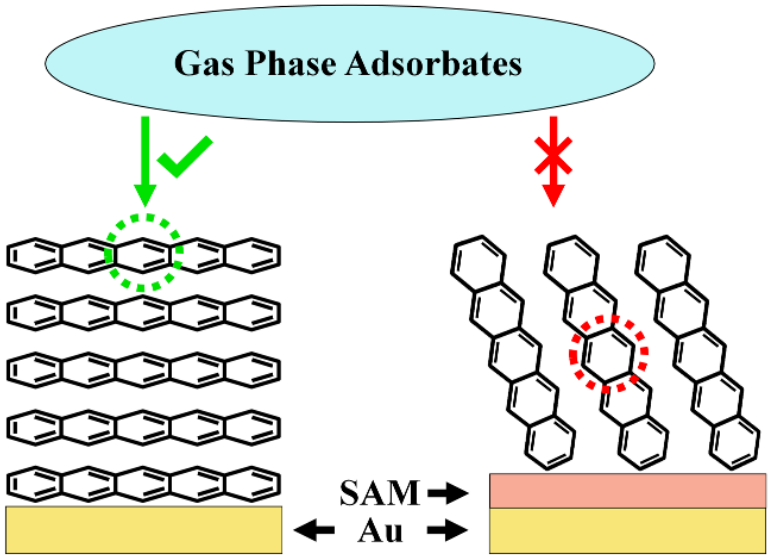


Figure 11. Highly orientation dependent access to reactive portions of pentacene thin films (dashed circles). (Left) Pentacene molecules on bare gold adopt a facedown configuration and adsorbates can freely approach the most reactive central ring for chemisorption. (Right) Pentacene on self-assembled monolayers (SAMs) adopts an upright configuration inhibiting adsorbate approach to any reactive π-system.

Fortunately, an unreactive crystal surface does not negate the possibility of reaction on thin films because structural defects (grain boundaries, dislocations, surface vacancies, step edges, and stacking faults) can have a profound influence on reactivity. Defects introduce a break in the crystallographic lattice, whether large in the case of grain boundaries, or atomic in the case of surface vacancies. When harnessed, defects can then trigger a broad collection of reactions. For example, the dissociative chemisorption of small molecules ($H_2O$, CO, $CO_2$, $SO_2$, $CH_3OH$, $CH_2CH_2$) is facilitated via surface defects, specifically oxygen surface vacancies on metal oxides.[80,81] Though the mechanism would be dramatically different for organic surfaces (i.e. pentacene), the general prominence of defect-induced chemistry prompted us to examine if the surface chemistry of organic films may also be influenced by defects and, if so, allow us to react a pentacene (001) surface.

As the defect density is very high in pentacene thin films,[82] if properly harnessed, defects

have the potential to facilitate Diels-Alder functionalization. Defects produce structural discontinuities in the crystal lattice and these render the nearby molecules more reactive by expanding the surrounding void.[83,84] The formed voids in the film serve as potential loci for the adsorbate molecules to position themselves in the correct transition state geometry for reaction, and can also accelerate adsorbate diffusion into the film[61] to reach an unreacted portion of the molecular surface. These effects are likely amplified by the nature of the organic reaction: formation and buildup of product at the reacting surface induces strain and causes the formation of further defects which accelerates reaction propagation throughout the film or crystal. Strain induced propagation through organic crystals has some precedence in the form of self-rearrangement of oxime picryl ethers.[83] All told, the defect-mediated approach seems especially amenable to the reactivity of an organic film.

Herein, we examine the reaction of pentacene thin films with vapor phase adsorbates via Diels-Alder chemistry to study the defects associated with grain boundaries and their ability to initiate reactivity. Utilizing the substrate's temperature during pentacene film formation to alter average crystal grain size, we observe reactivity that is highly correlated. These results are then extended onto single crystal systems that are grown with one to two domain boundaries, where defect-induced reaction propagation can be observed. This defect-mediated mechanism demonstrates the viability of surface functionalization on heretofore unreactive surface orientations, and thus the viability of Diels-Alder chemistry towards improving OTFTs.

## Experimental Section

### Materials

All evaporation metals are of 99.9% or greater purity. Sublimed grade pentacene and tetracene, *N*-methylmaleimide, 1-dodecanethiol, and 200 proof ethanol (ACS grade) were

commercially obtained and used without further purification.

**Preparation of Gold Substrates**

Rectangular cut Si(111) wafers were first cleaned in piranha solution (3:1, $H_2SO_4$: $H_2O_2$) for 30 min. The wafers were rinsed with copious amounts of 18 MΩ•cm water, sonicated for 20 min, and dried under a stream of nitrogen. Wafers were then mounted in a thermal evaporator (Kurt J. Lesker NANO38). A 5 nm chromium adhesion layer was deposited, followed by 50 nm of silver and 50 nm of gold at a base pressure of $<1\times10^{-6}$ Torr and a deposition rate of 1 Å/s.

**Self-Assembly of 1-Dodecanethiol onto Gold Substrates**

Self-assembled monolayer (SAM) decorated gold substrates were prepared by submerging the freshly prepared gold substrates in a nitrogen purged 200 proof ethanolic solution of ~1 mM 1-dodecanethiol for 24 h at room temperature. After the self-assembly, the substrates were rinsed with copious amounts of ethanol, sonicated, rinsed an additional time with ethanol, and dried under a stream of nitrogen. SAM thicknesses were assessed through ellipsometry measurements after the self-assembly (Gaertner Scientific LSE Stokes Ellipsometer with 632.8 nm laser). The surface thickness was modeled as a single absorbing layer atop an infinitely thick substrate (fixed $n_s$) and the index of refraction was set to 1.45. Following thickness measurements, the SAM substrates were carefully cut in half to generate a witness portion for microscopy, and a consumable portion for reaction. Both parts were rinsed with ethanol, sonicated, rinsed again, and then dried under a stream of nitrogen.

**Pentacene Thin Film Deposition**

40 nm pentacene thin films were deposited using a home-built sublimation chamber, with a source to substrate distance of 16–17.5 cm, at a rate of 0.05 Å/s. Pentacene was sublimed from a resistively heated cartridge onto SAM decorated gold substrates at a base pressure of $2\times10^{-6}$

Torr. During sublimation, the substrate temperature was controlled with a home-built resistive heating element which allowed a temperature differential to be maintained between two samples (Figure S9). Thicknesses of the films were monitored using a quartz crystal microbalance (INFICON SQM-160).

**Measurement of Grain Structure**

Witness samples were analyzed via atomic force microscopy (AFM; MFP 3D microscope, Asylum Research, Santa Barbara, CA, USA). AFM measurements were performed in tapping (noncontact) mode using a diamond-like-carbon coated AFM tip (Tap190DLC, Budget Sensors, Sofia, Bulgaria). The average grain size and total projected grain boundary length in each image was determined using AFM software (Gwyddion 2.5), whereby grains were marked by segmentation followed by measurements using 100 iterations of line-cut method.

**Growth of Tetracene Crystals**

Tetracene crystals were grown onto gold coated Si(111) substrates using a home-built physical vapor transport tube furnace that was 95 cm in length and had a temperature gradient of approximately ~2 °C/cm in the growth zone (Figure S10).[85] 100 mg of tetracene source material were heated to 225 °C under a flow of ultra-high purity argon (40 mL/min). The crystals were collected from the region of the furnace at 205 °C after 48 h. The gold substrate with crystals was imaged before reaction with a Hitachi SU-3500 scanning electron microscope (SEM) at 5 kV.

**Diels-Alder Reaction of Acene Surfaces**

The acene samples and a small vial of approximately 8 mg of *N*-methylmaleimide were placed at opposite ends of a Schlenk tube under nitrogen. The samples were heated to 50 °C (pentacene films) or 80 °C (tetracene crystals) for 18 h. The reaction was quenched by insulating

the substrate end of the Schlenk tube while cooling the opposite end with dry ice to condense residual *N*-methylmaleimide vapors. As an additional measure to remove physisorbed *N*-methylmaleimide, acene samples were further subjected to high vacuum conditions ($<5.5\times10^{-6}$ Torr) for at least 1 h. The extent of reaction on the thin films was evaluated by PM-IRRAS (Bruker Optics Tensor 37 with a PMA50 accessory and a liquid nitrogen cooled MCT detector). Spectra were taken at a resolution of 2 $cm^{-1}$. The extent of reaction on the surface was determined by the intensity of absorptions associated with adduct formation (1700 and 1280 $cm^{-1}$).[39] Reactions on crystal surfaces were qualitatively evaluated via comparison of SEM images before and after reaction.

## Results and Discussion

Defects are intrinsic to pentacene film growth and a tally of them is critical to forming an effective hypothesis concerning their role in reactivity. Typical pentacene thin films have on the order of $10^{11}$ dislocations/$cm^2$,[82] significantly more single vacancies,[86] and assuming an average grain size of about 500 nm, roughly $10^8$ grain boundaries per $cm^2$. All are expected to impact reactivity, as each provides a means for adsorbates to reach the recessed acene core (Figure 1, right). While dislocations and vacancies are numerically attractive, they are challenging to control and thus they were not used to benchmark against reactivity. Though grain boundaries occur far less, their relative importance is outsized as this type of defect is large in size and also influences derivative defect (dislocation and vacancy) formation.[82,86–88] Indeed, grain boundaries are not reflective of merely being two domains meeting, but rather, the height change from edge to center implies additional step edges (roughly 30 for the films below). There is also a high degree of compressive stress at grain boundaries, and this interferes with ideal crystal geometry growth: dislocation formation is amplified under strain.[87] Due to both the ease with which they

can be controlled, and their interrelationship with other defects, grain boundaries (and average grain size) are used to study how surface defects can impart reactivity to the thin-film phase of pentacene.

The average size of pentacene grains can be controlled via two methods: substrate control and thermal control. In the first method, self-assembled monolayers (SAMs) coat the underlying substrate and the SAM chain can control the nucleation density of the pentacene thin film. Longer SAMs have been hypothesized to generate significantly more nucleation sites for crystalline domains, resulting in smaller grains.[89] Several classes of SAMs have displayed this relationship between SAM chain length and pentacene grain size, including thiols,[90] silanes,[91,92] phosphonic acids,[93–95] and carboxylic acids.[96] In the second method, an elevated substrate temperature effectively lowers the activation energy for surface diffusion,[97,98] thereby allowing pentacene molecules to diffuse more rapidly on the surface and minimizing nucleation of new crystals.[99] This in turn facilitates the formation of larger crystalline grain sizes. Recent studies[100,101] have demonstrated a range of grain sizes of pentacene can be produced by controlling the temperature of the substrate during film formation.

Although there are several reports outlining the success of using SAMs as a means to control pentacene grain size, in our hands we found results to be highly varied. In contrast, thermally activated grain growth proved to be simple and robust. Grain size differentials were pronounced between the two different temperature samples, with nearly 425% larger average grain size when going from a substrate temperature of 30 to 60 ºC. The large difference in average grain size between the two temperature samples will greatly simplify the comparison between reactivity and defect density. Of additional merit, the batch to batch variability was low. At the temperatures evaluated, the average grain size varied by less than 100 nm (25%) between

two sequential samples (Figure S11).

The aforementioned films were produced by depositing pentacene on 1-dodecanethiol coated gold substrates, a SAM being critical to generating thin-film phase pentacene. The quality of the SAM was evaluated via surface order and thickness. The $\nu_{CHa}$ and $\nu_{CHs}$ peak positions in the IR spectra indicate the ordering of the alkane chain within the monolayer. These two peaks appear at 2920 and 2852 $cm^{-1}$ for 1-dodecanethiol, respectively matching literature values within 2 $cm^{-1}$ (Figure S12).[102] For ellipsometry, the thickness of the 1-dodecanethiol SAMs was 19 Å, which is consistent with previous reported thicknesses (18 Å).[62,103] Following pentacene deposition on the SAM, the orientation of pentacene was determined using the relative infrared peak intensities at 1445, 1164, 910, and 731 $cm^{-1}$; sets of vibrations that are orthogonal to one another. When pentacene within the film is oriented perpendicular to the gold surface (e.g. in a (001) film), the vibrations at 1445 and 1164 $cm^{-1}$ are amplified while the normally dominant peaks at 910 and 731 are diminished[69] due to the surface selection rules.[104] IR spectra for the films are reported in Figure 12, and their IR absorptions confirm a nominally (001) film, i.e. the long axis of the pentacene is ~22º from the surface normal (Figure 11, right).

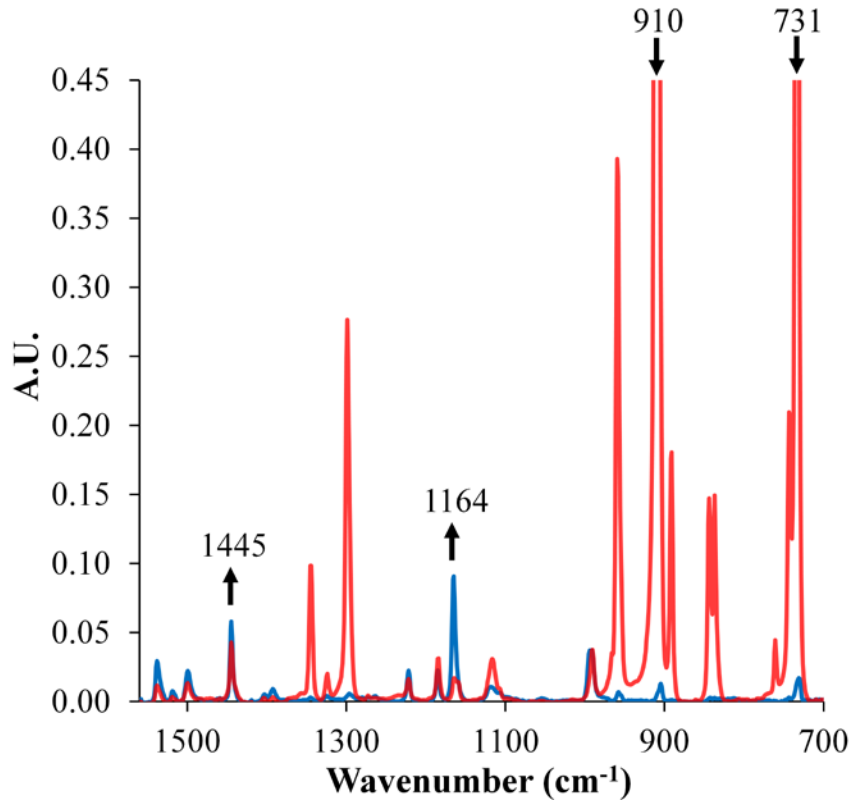


Figure 12. PM-IRRAS spectra of pentacene on bare gold (red; peaks are clipped for 910 and 731 $cm^{-1}$, but reach a maximum of 2.6 and 1.7 A.U.) and on 1-dodecanethiol (blue). Arrows at 1445, 1164, 910, and 731 $cm^{-1}$ indicate the direction of the peak intensity change in going from pentacene on bare gold to a nominally (001) film.

AFM images (Figure 13) of the pentacene films reveal two very different grain sizes for the room temperature sample (400 ± 200 nm) and the one at elevated temperatures (1700 ± 800 nm for 60 °C), consistent with previously mentioned reports.[100,101] Further analysis of the AFM data (Figure 13c and d) indicates that the overall structure of each domain is similar, with rough terraces seen in both samples, and small vacancies (equivalent to ~2 nm thickness, or about two molecules of thickness) seen across the terraces. Because the average exposed area of the side surface is the length of the total grain boundary length times the film thickness, the total grain boundary length can be used to represent the average defect area of the films with the same thickness. For the samples in Figure 13, this is 226 μm vs 68 μm or a 3.3-fold difference. Since

the defect density on the room temperature substrate is so markedly higher, if defects do play a critical role in reactivity, these two samples should have dramatically different reactivity; it also remains to be seen if the defects in either sample are sufficient to render this surface reactive on the timescale of this experiment.

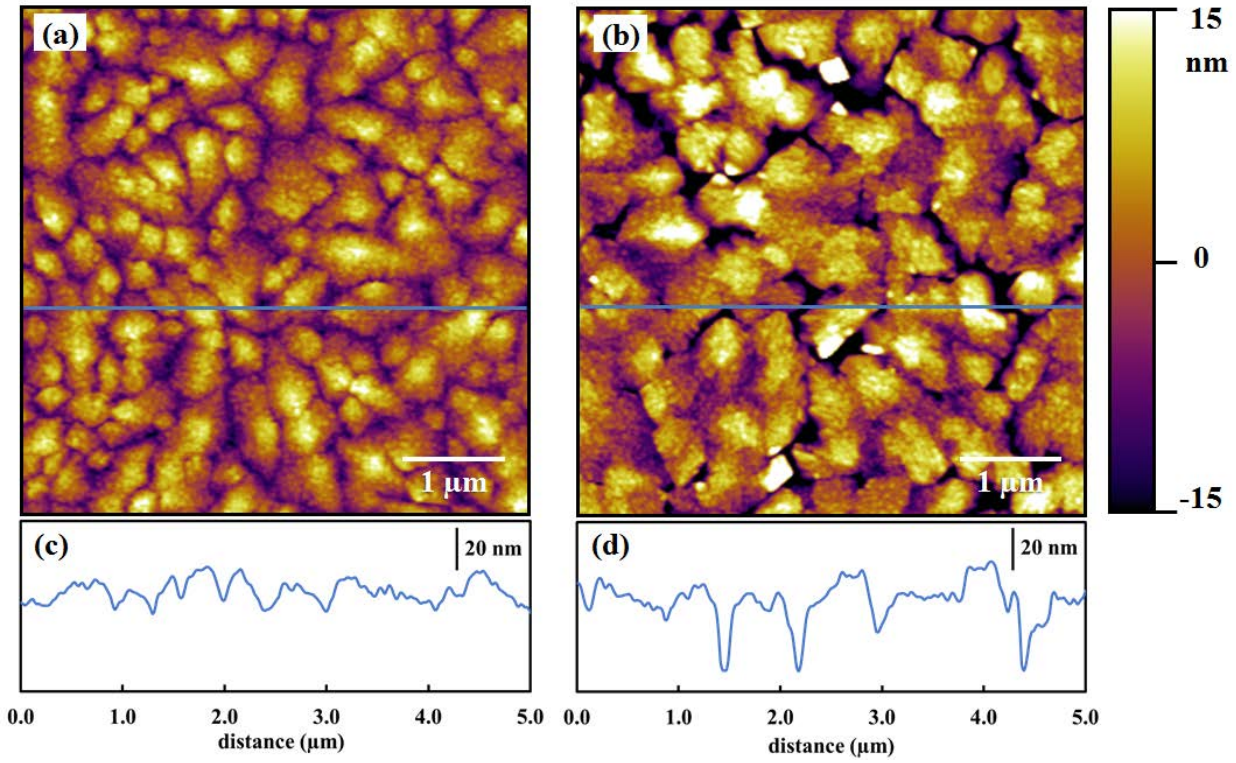


Figure 13. Grain structure of 40 to 50 nm thick pentacene thin films sublimed onto 1-dodecanethiol decorated gold substrates at a) room temperature and b) 60 °C. The AFM images (5×5 µm) were taken in non-contact mode. Line scans across the c) room temperature substrate and d) 60 °C substrate.

The reaction of pentacene films was accomplished by heating the substrate in the presence of vapor phase *N*-methylmaleimide for 18 h at 50 °C. IR analysis of these films reveals the growth of new infrared peaks at 1700 $cm^{-1}$ and 1280 $cm^{-1}$. These peaks suggest that an effective Diels-Alder reaction has taken place on the pentacene film (Figure 14). It is remarkable that the pentacene (001) surface is reactive, and this will be discussed in further detail later. But

the greater point is that the reactivity of each film is highly correlated to the projected grain boundary length which demonstrates that the defects are the likely source of this reactivity. Specifically, the room temperature sample (boundary length = 226 μm) has reacted significantly faster than the 60 ºC sample (boundary length = 68 μm). While the data correlation appears semiquantitative, with a 3.3-fold increase in boundary length generating a 3 to 4-fold increase in reactivity, we caution against over quantifying the relationship as some samples had lower reactivity differences (Figure S13). However, when one considers the lack of reactivity in single crystal samples,[46] a direct relationship is evident. Another aspect of this data is that peak intensities are near or above what would be expected for reacting a monolayer's worth of material with the pentacene film. This suggests that the reaction is not confined to the grain boundaries, rather, the boundaries act as a site from which reaction can propagate across the surface and into the subsurface.

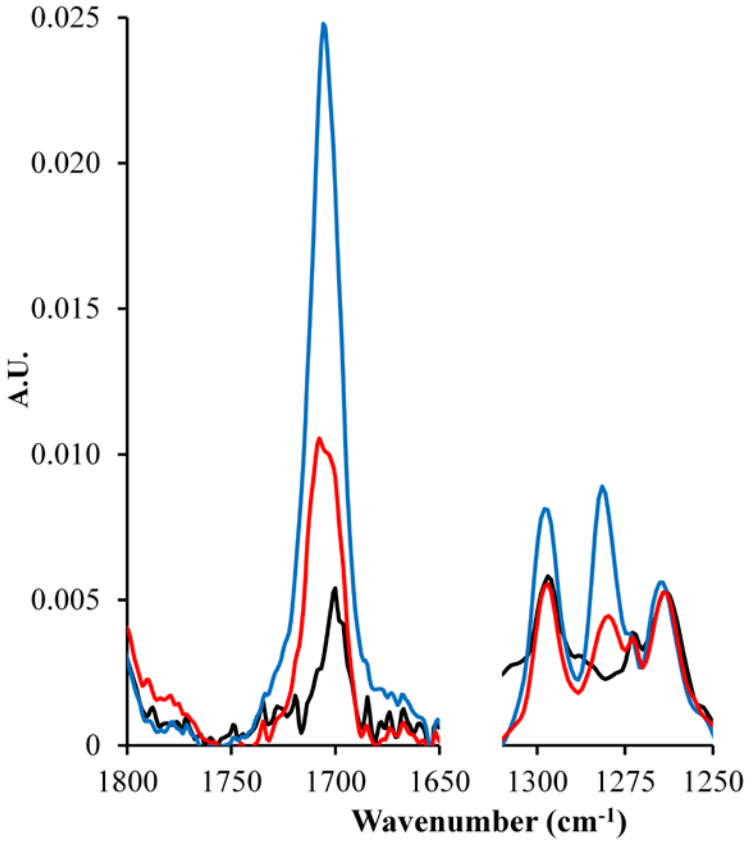


Figure 14. PM-IRRAS spectra comparing reactivity of pentacene films with *N*-methylmaleimide for 18 h at 50 °C. The color scheme is as follows: unreacted pentacene (black), reaction of pentacene films prepared at 60 °C (red), and reaction of pentacene films prepared at room temperature (blue).

We wish to reemphasize the significance of being able to react the imperfect (001) pentacene surface. Previously, the exposure of tetracene crystals to Diels-Alder reaction conditions revealed the main face, (001), was unreactive.[46] In our work, with milder conditions, pentacene films with intrinsically high defect density resulted in significant reaction at the surface. More importantly, results showing monolayer or greater coverage implies that the reaction may be propagating across the surface. This relationship compelled us to examine if propagation from a small amount of defects could render the (001) surface of a *crystal* reactive. To explore this phenomenon more fully, and for direct evidence of this propagation, reaction on

a surface that is predominantly defect-free is required.

Tetracene crystals were grown from the vapor phase in a manner similar to Laudise. They are, on average, larger than 50 µm in size and have well-defined crystal faces. Scanning electron microscopy (SEM) was used to survey the crystals, and then locate crystals with only one or two significant defects on the surface. In Figure 15a, we isolated a single crystal with only one major defect on the surface: a line originating from the bottom of the hexagonal crystal and continuing through roughly a quarter of the crystal (indicated by arrows). If the propagation of adsorbates is indeed occurring, one should be able to observe its dispersal from this feature. This experiment is made simpler by the fact that reaction with *N*-methylmaleimide has been reported to induce small asperities on the surface,[47] and hence reaction progress can be imaged directly via SEM.

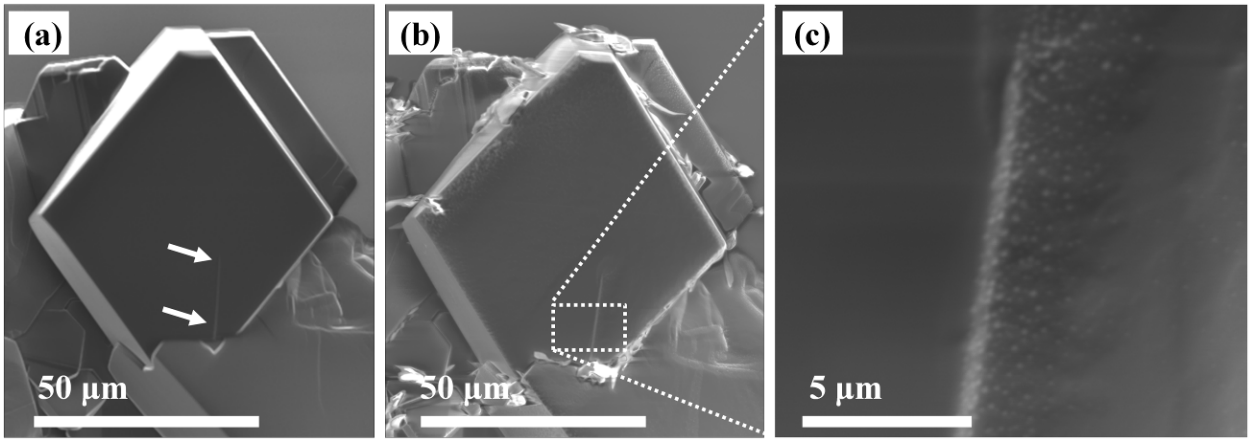


Figure 15. SEM images of tetracene crystals a) before reaction and b) after reaction with *N*-methylmaleimide. The white arrows indicate the dislocation defect on the surface. c) Magnified region displaying reaction propagation.

The crystals were exposed to *N*-methylmaleimide vapor at 80 °C for 18 h. The temperature was chosen based on prior evidence that the largest face of the tetracene crystals was inert at 80 °C. The exposed crystals were re-examined with SEM to locate asperities indicative of reaction. Indeed, the images (Figure 15b and c) show adduct formation in the vicinity of the dislocation step, and importantly, the reaction appears to have propagated outward from the

dislocation site. Analysis on additional tetracene crystals with dislocation defects demonstrate that this reaction propagation is representative (Figure S14). The reaction can be tracked as far as 3 μm from the nucleation site, with the product amount diminishing as a function of distance from the defect. Thus reactivity is not confined to the immediate vicinity of the defect. Additionally, the reaction's progression appears unidirectional (only to the right) from the defect. This is noteworthy as it suggests the adsorbate propagation initiates through the higher terrace within the dislocation. These results suggest that the defects not only play a role in the initiation of the reaction, but are also are important in the propagation of reaction.

## Conclusions

In conclusion, the influence of defects on the reactivity of organic films was evaluated by performing the Diels-Alder reaction on what is nominally a pentacene (001) surface. By controlling defect density between samples via a temperature differential, reaction rates were correlated to higher defect density. In the context of previously reported inertness of a tetracene (001) surface, this reactivity indicates that defects are critical to reaction of this molecular orientation. This understanding was transitioned from a collection of defects to a direct observation of a single defect's influence on reactivity by studying reaction propagation from a dislocation in a single crystal. Results confirm the reaction is not confined to the immediate vicinity of the defect, but can propagate for microns across the crystal surface. Together, these results demonstrate the ability to react thin-film phase pentacene, and even the (001) surface of minimally flawed single crystals. These results represent a significant step towards improving the organic interface in top-contact OTFTs.

# APPENDIX A

# SUPPLEMENTAL INFORMATION FOR CHAPTER TWO

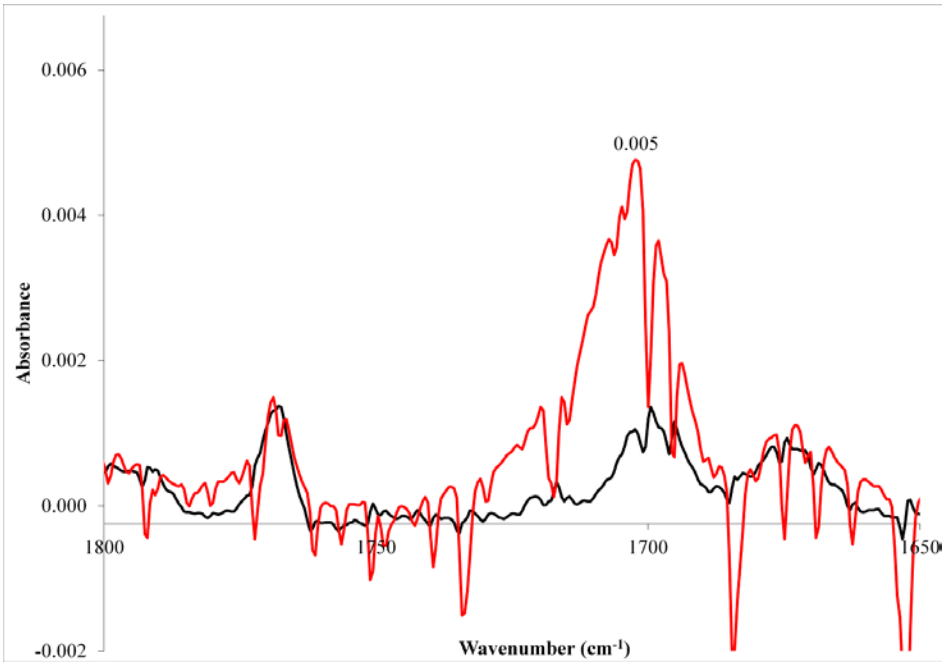


Figure S1. IRRAS spectrum of a pentacene reaction with *N*-methylmaleimide at 25 °C for 24 h. The color scheme is as follows: pristine pentacene (black), 25 °C reacted pentacene (red). The absorbance is appropriate for a monolayer regime of material.[70]

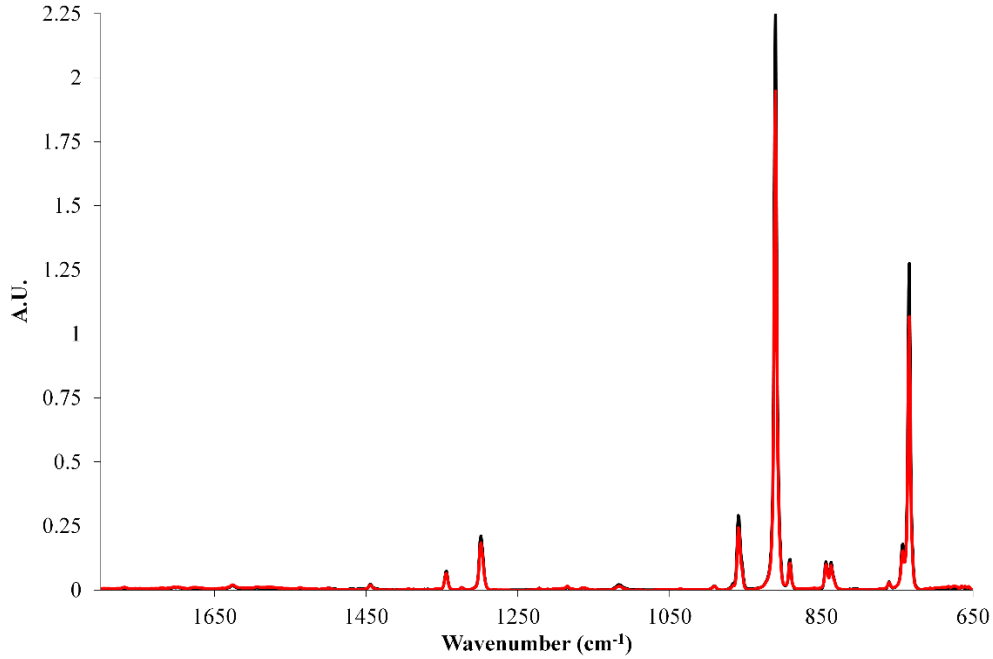


Figure S2. PM-IRRAS spectra of a 75 °C heated pentacene substrate after 24 h. The color scheme is as follows: pristine pentacene (black), 75 °C heated pentacene (red).

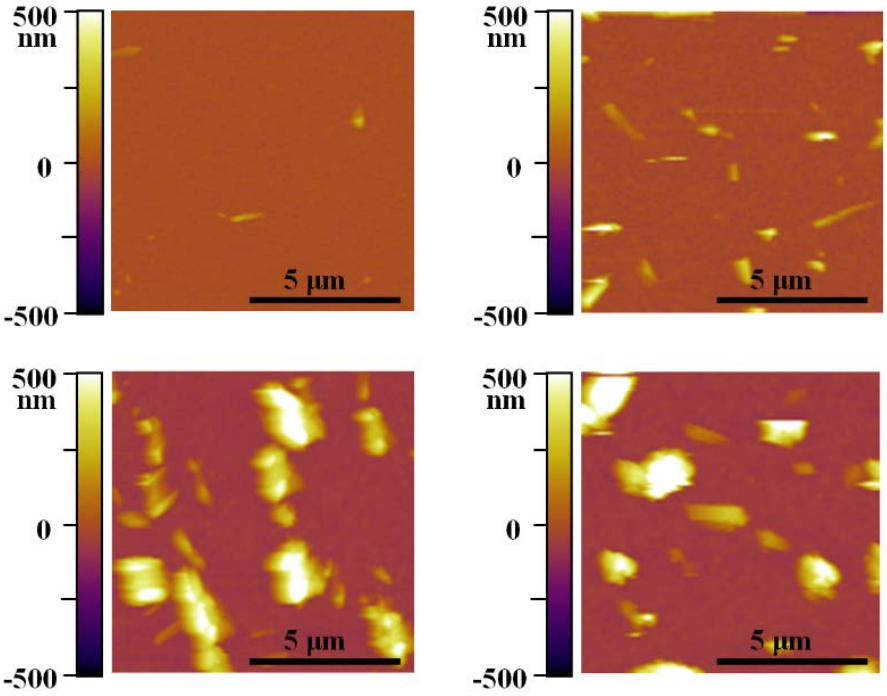


Figure S3. AFM images of pentacene substrates reacted with *N*-methylmaleimide for 24 h. The reaction temperatures are as follows: top left (25 °C), top right (35 °C), bottom left (40°C), bottom right (65 °C).

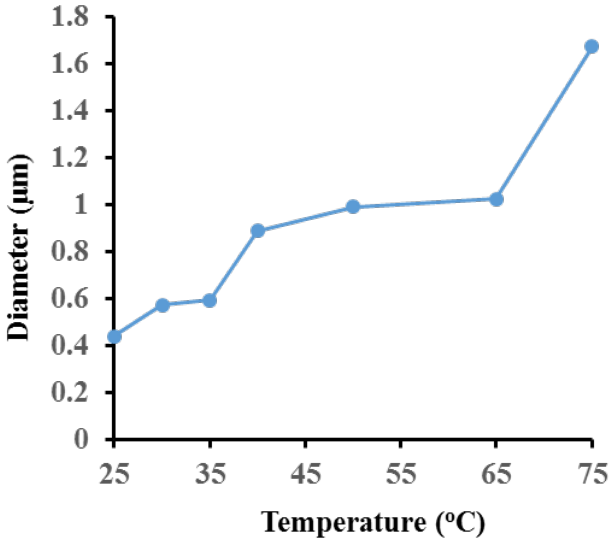


Figure S4. AFM measurements of average diameter of surface protrusions over a 400 µm$^2$ area on pentacene substrates reacted with *N*-methylmaleimide for 24 h from 25 to 75 ° C. Features accounted for here are under the restraint of a protrusion height threshold of 3 times the RMS of the area between the protrusions (see **Figure S5**).

Table S1. The rms roughness was measured of 20 × 20 μm AFM images using bootstrap analysis for the reaction of *N*-methylmaleimide with pentacene thin films (24 h, multiple temperatures). The average of these values at each temperature comprise the rms roughness plot in Figure 8.

| **Temperature, °C** | **rms Roughness, nm** |
|---|---|
| Pristine Pentacene | 5.20 |
| 25 | 23.04 |
| | 16.87 |
| | 17.11 |
| | 13.97 |
| 30 | 32.46 |
| | 40.09 |
| | 40.40 |
| | 38.75 |
| 35 | 77.61 |
| | 69.84 |
| | 62.73 |
| | 54.38 |
| 40 | 124.35 |
| | 127.14 |
| | 143.74 |
| | 134.41 |
| 50 | 154.52 |
| | 175.05 |
| | 149.84 |
| | 143.86 |
| 65 | 148.04 |
| | 171.16 |
| | 163.53 |
| | 135.69 |
| 75 | 513.57 |
| | 457.82 |
| | 370.11 |
| | 309.83 |

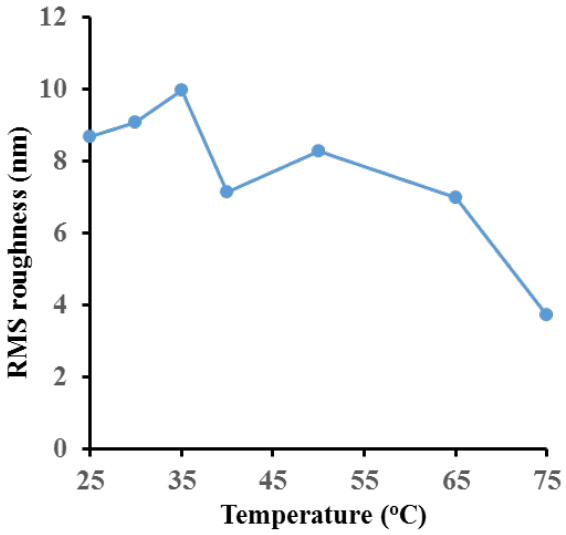


Figure S5. AFM measurements of rms roughness in-between surface protrusions for pentacene substrates reacted with *N*-methylmaleimide for 24 h from 25 to 75 ° C.

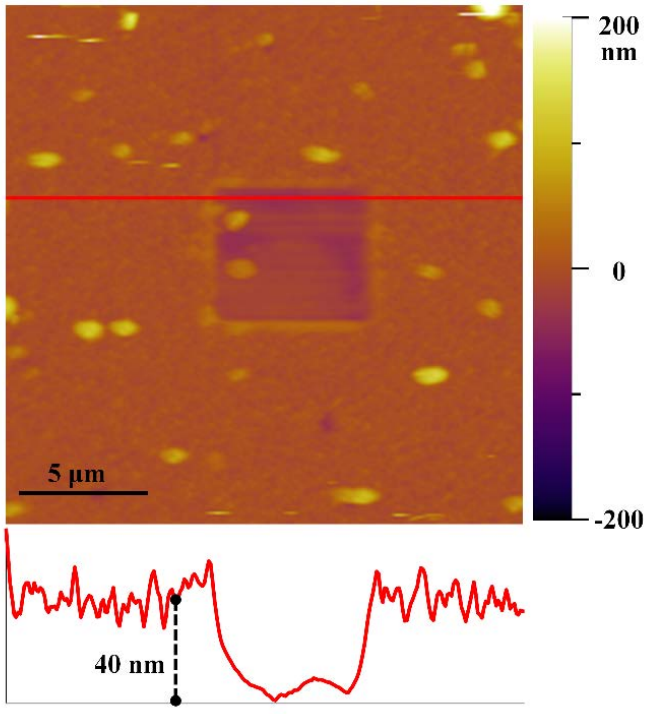


Figure S6. AFM image of a pentacene substrate reacted with *N*-methylmaleimide at 50 °C for 24 h. A line scan across a scratched square area of the sample shows a continuous thin film exists under the surface protrusions.

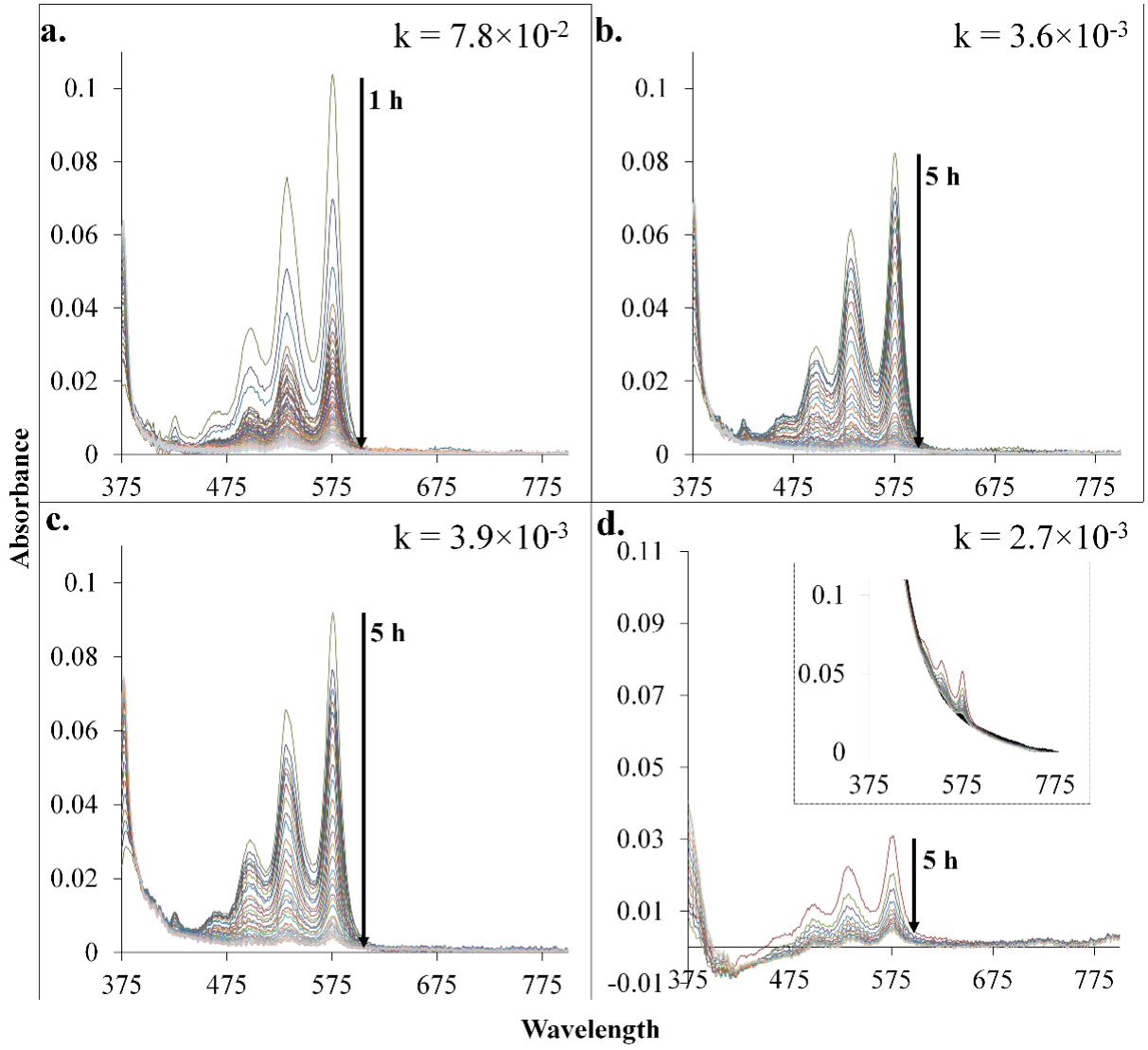


Figure S7. The UV-vis spectra (in chloroform) of the reaction between pentacene and adsorbate molecules (*N*-methylmaleimide, a; maleic anhydride, b; maleimide, c; tetrafluorobenzoquinone, d) at 23 °C are shown. All spectra are after subtraction of the absorbance of the adsorbate/dienophiles. The rates, k ($M^{-1}s^{-1}$), are displayed for each reaction in the upper portion of the UV-vis spectra.

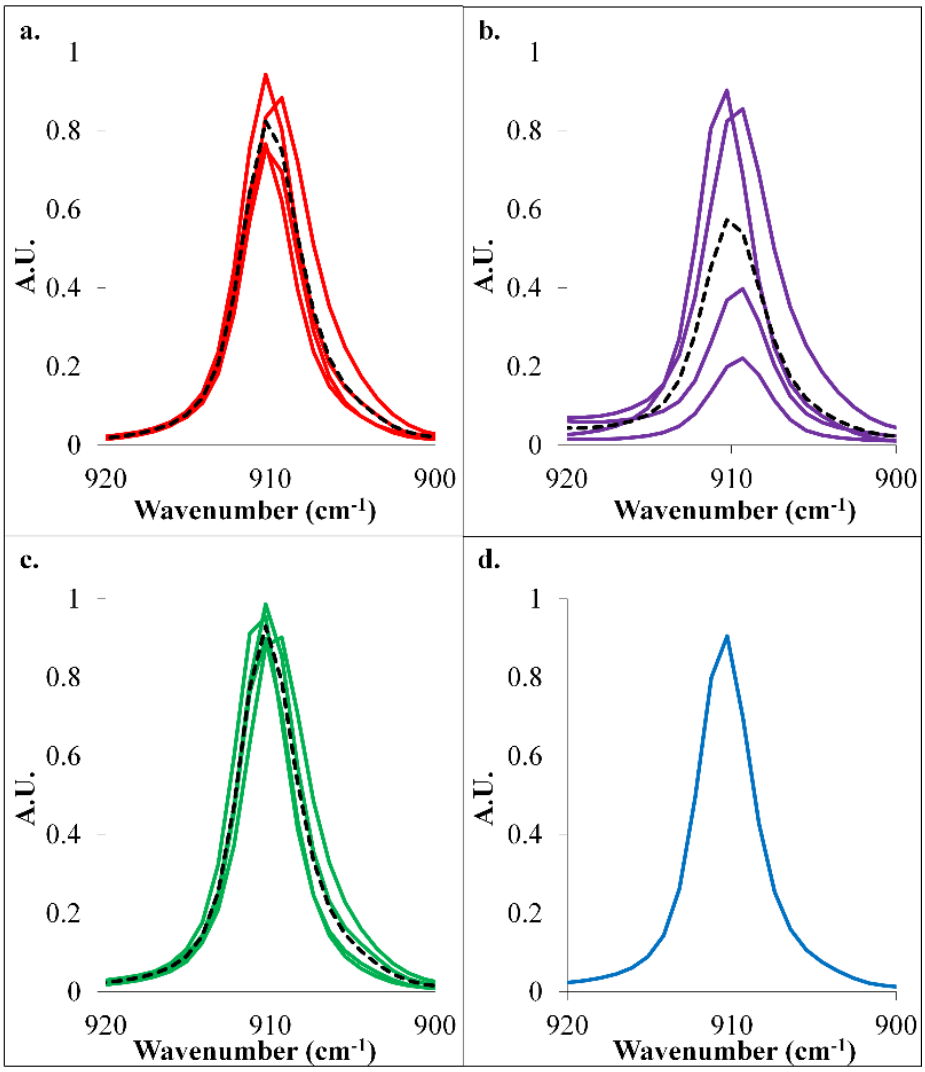


Figure S8. The reaction between pentacene thin films and adsorbates (*N*-methylmaleimide, red; maleic anhydride, purple; tetrafluorobenzoquinone, green; maleimide, blue) were monitored with PM-IRRAS. Reactions with *N*-methylmaleimide, maleic anhydride, and tetrafluorobenzoquinone were repeated 4 times. To account for the A.U. variability at 910 $cm^{-1}$ for the multiple thin-films used, all spectra here were normalized and rescaled and are shown above. Also included is the average of the normalized spectra (dashed curve) with error bars showing the standard deviation (*N*-methylmaleimide, 0.2; maleic anhydride, 0.8; tetrafluorobenzoquinone, 0.1).

# APPENDIX B

# SUPPLEMENTAL INFORMATION FOR CHAPTER THREE

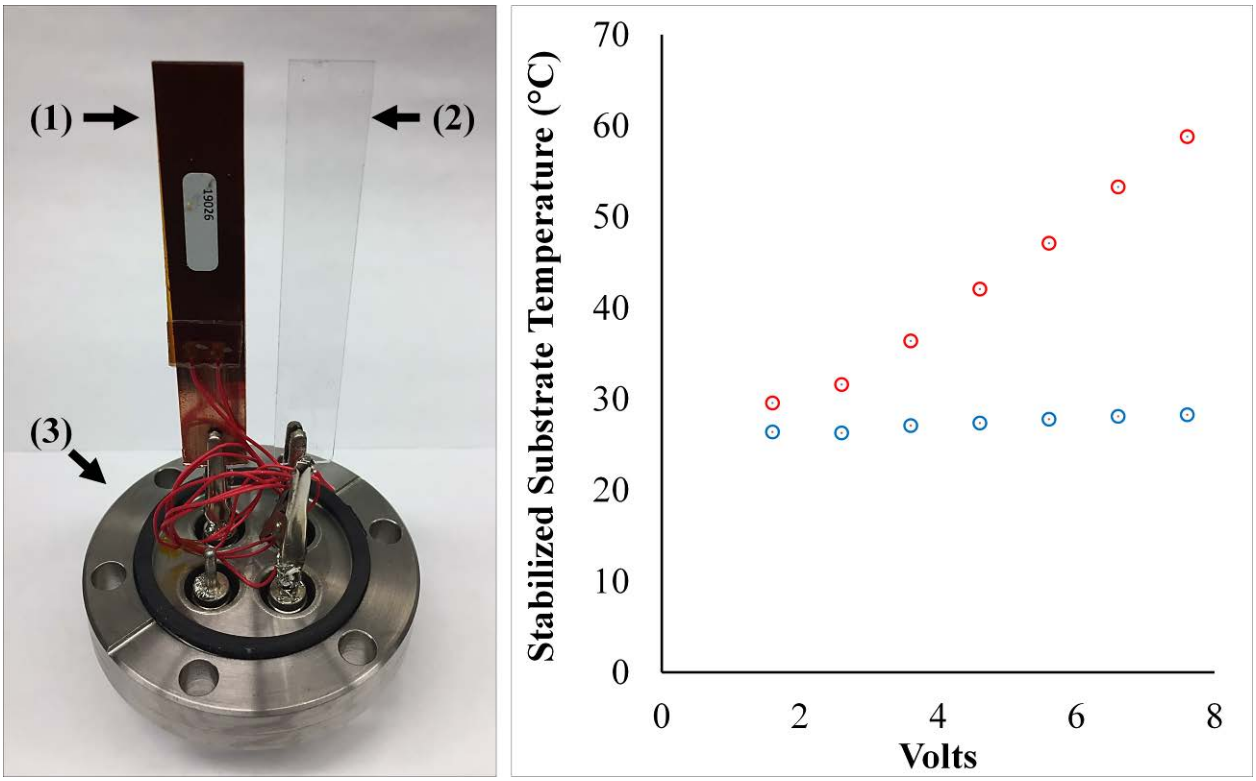


Figure S9. Left: Image of the controlled temperature stage. (1) Copper support with a resistively heated element adhered to the backside of the support. (2) Glass support. (3) CF flange with 4 BNC feedthroughs. Right: Calibration curve for the heated (red) and non-heated (blue) supports. Temperature was measured with a type K thermocouple at $4.5\times10^{-6}$ Torr after the temperature stabilized for 30 minutes.

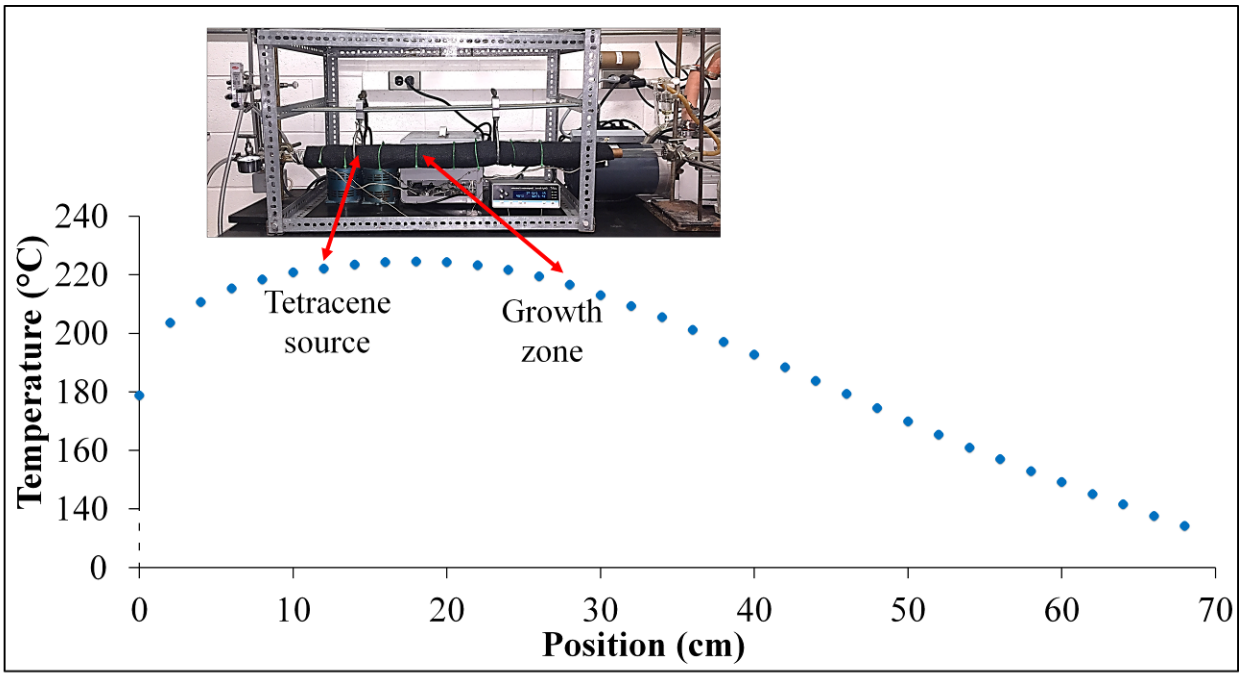


Figure S10. Temperature profile at positions across the physical vapor transport tube furnace with an inset image highlighting source and growth zones.

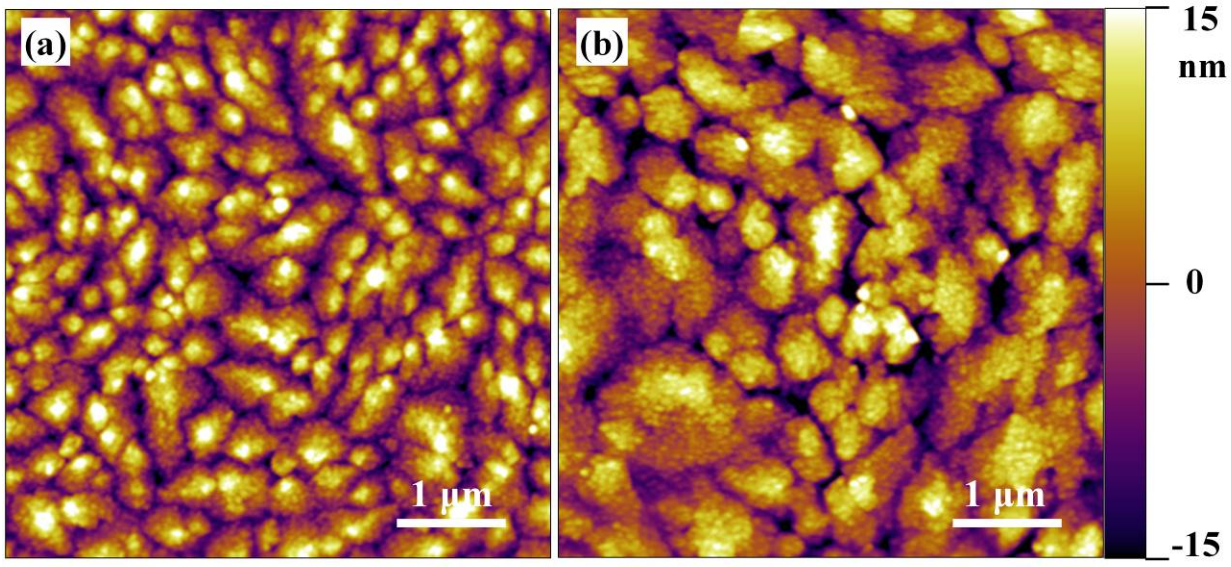


Figure S11. AFM images of additional samples of pentacene films formed at a) room temperature and b) 60 °C have average grain sizes of 300 ± 200 and 1700 ± 800 nm and total grain boundary lengths of 281 and 56 µm, respectively.

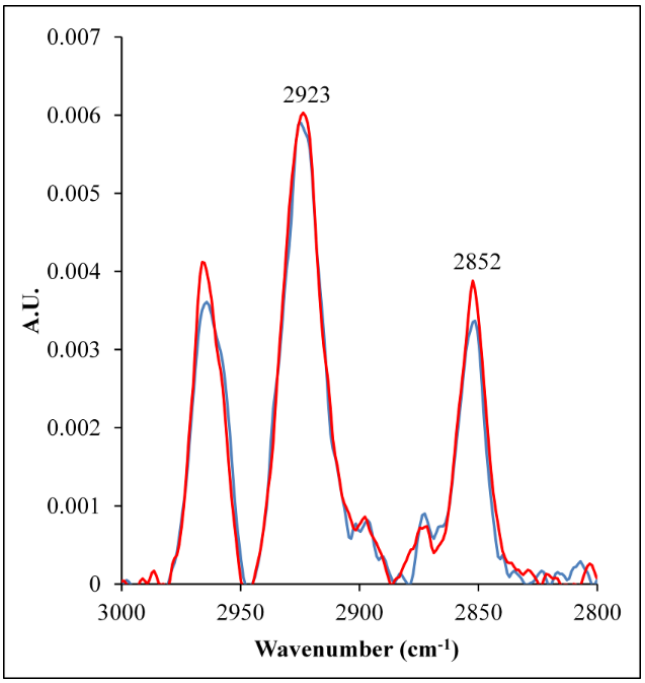


Figure S12. PM-IRRAS spectra of pentacene on 1-dodecanethiol self-assembled monolayer for samples utilized in Figure 2 (red and blue).

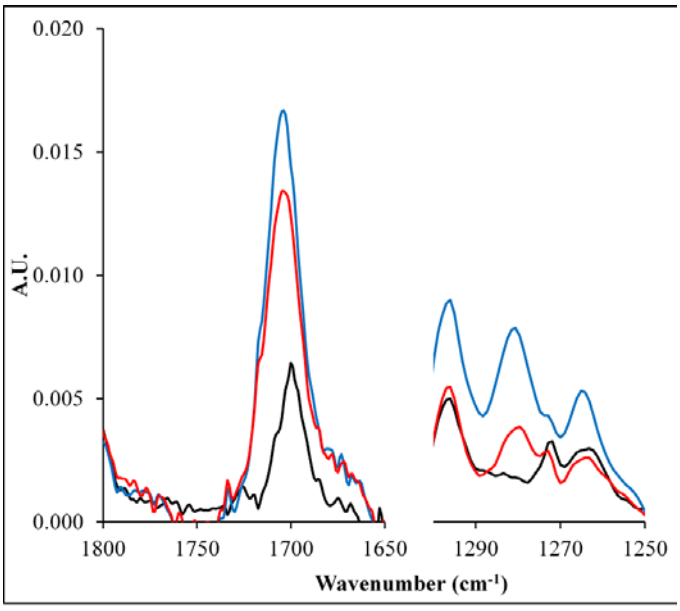


Figure S13. PM-IRRAS spectra for additional samples of pentacene reacted with *N*-methylmaleimide for 18 h at 50 °C. The color scheme is as follows: unreacted pentacene (black), reaction of pentacene films prepared at 60 °C (red), and reaction of pentacene films prepared at room temperature (blue).

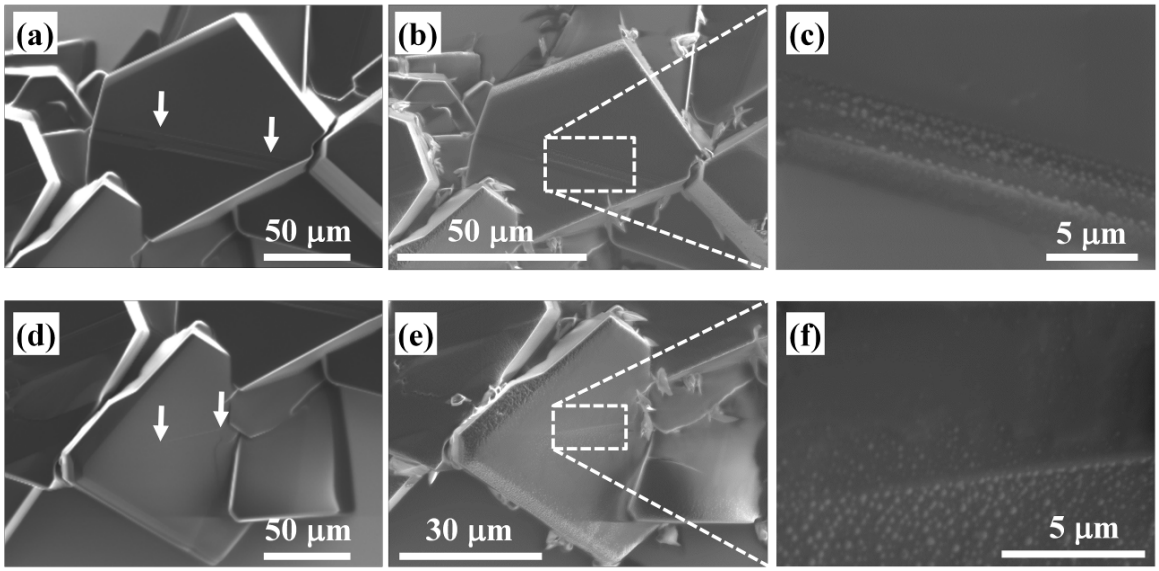


Figure S14. SEM images of additional tetracene crystals a,d) before reaction and b,e) after reaction with *N*-methylmaleimide. The white arrows indicate the dislocation defect on the surface. c,f) Magnified region displaying reaction propagation.

REFERENCE LIST


(1) Mertens, R. *The OLED Handbook : A Guide to OLED Technology, Industry & Market*; OLED-Info, 2013.

(2) Gather, M. C.; Köhnen, A.; Meerholz, K. White Organic Light-Emitting Diodes. *Advanced Materials* **2011**, *23* (2), 233–248.

(3) Tao, Y.; Yang, C.; Qin, J. Organic Host Materials for Phosphorescent Organic Light-Emitting Diodes. *Chem. Soc. Rev.* **2011**, *40* (5), 2943–2970.

(4) Kulkarni, A. P.; Tonzola, C. J.; Babel, A.; Jenekhe, S. A. Electron Transport Materials for Organic Light-Emitting Diodes. *Chemistry of Materials* **2004**, *16* (23), 4556–4573.

(5) Chen, C.-T. Evolution of Red Organic Light-Emitting Diodes: Materials and Devices. *Chemistry of Materials* **2004**, *16* (23), 4389–4400.

(6) Hedley, G. J.; Ruseckas, A.; Samuel, I. D. W. Light Harvesting for Organic Photovoltaics. *Chemical Reviews* **2017**, *117* (2), 796–837.

(7) Sun, S.-S.; Sariciftci, N. S. *Organic Photovoltaics: Mechanisms, Materials, and Devices*; Optical Science and Engineering; CRC Press, 2017.

(8) Leo, K. Organic Photovoltaics. *Nature Reviews Materials* **2016**, *1*, 16056.

(9) Mazzio, K. A.; Luscombe, C. K. The Future of Organic Photovoltaics. *Chem. Soc. Rev.* **2015**, *44* (1), 78–90.

(10) Wallace, C. H. C. *Organic Solar Cells: Materials and Device Physics*; Green Energy and Technology; Springer-Verlag London, 2013.

(11) Wang, C.; Dong, H.; Hu, W.; Liu, Y.; Zhu, D. Semiconducting π-Conjugated Systems in Field-Effect Transistors: A Material Odyssey of Organic Electronics. *Chemical Reviews* **2012**, *112* (4), 2208–2267.

(12) Braga, D.; Horowitz, G. High-Performance Organic Field-Effect Transistors. *Advanced Materials* **2009**, *21* (14–15), 1473–1486.

(13) Logothetidis, S. Flexible Organic Electronic Devices: Materials, Process and Applications.

*Materials Science and Engineering: B* **2008**, *152* (1), 96–104.

(14) Muccini, M. A Bright Future for Organic Field-Effect Transistors. *Nat Mater* **2006**, *5* (8), 605–613.

(15) Sirringhaus, H. Device Physics of Solution-Processed Organic Field-Effect Transistors. *Advanced Materials* **2005**, *17* (20), 2411–2425.

(16) Lim, J. A.; Lee, W. H.; Lee, H. S.; Lee, J. H.; Park, Y. D.; Cho, K. Self-Organization of Ink-Jet-Printed Triisopropylsilylethynyl Pentacene via Evaporation-Induced Flows in a Drying Droplet. *Advanced Functional Materials* **2008**, *18* (2), 229–234.

(17) Aernouts, T.; Aleksandrov, T.; Girotto, C.; Genoe, J.; Poortmans, J. Polymer Based Organic Solar Cells Using Ink-Jet Printed Active Layers. *Applied Physics Letters* **2008**, *92* (3), 033306.

(18) Søndergaard, R. R.; Hösel, M.; Krebs, F. C. Roll-to-Roll Fabrication of Large Area Functional Organic Materials. *Journal of Polymer Science Part B: Polymer Physics* **2013**, *51* (1), 16–34.

(19) Krebs, F. C. All Solution Roll-to-Roll Processed Polymer Solar Cells Free from Indium-Tin-Oxide and Vacuum Coating Steps. *Organic Electronics* **2009**, *10* (5), 761–768.

(20) Kim, S.; Kwon, H.-J.; Lee, S.; Shim, H.; Chun, Y.; Choi, W.; Kwack, J.; Han, D.; Song, M.; Kim, S.; et al. Low-Power Flexible Organic Light-Emitting Diode Display Device. *Advanced Materials 23* (31), 3511–3516.

(21) Sekitani, T.; Zschieschang, U.; Klauk, H.; Someya, T. Flexible Organic Transistors and Circuits with Extreme Bending Stability. *Nat Mater* **2010**, *9* (12), 1015–1022.

(22) Sekitani, T.; Nakajima, H.; Maeda, H.; Fukushima, T.; Aida, T.; Hata, K.; Someya, T. Stretchable Active-Matrix Organic Light-Emitting Diode Display Using Printable Elastic Conductors. *Nature Materials* **2009**, *8*, 494.

(23) Das, R.; Ghaffarzadeh, K.; Chansin, G.; He, X. *Printed, Organic & Flexible Electronics Forecasts, Players & Opportunities 2017-2027*; IDTechEx, 2017.

(24) Hummer, K.; Ambrosch-Draxl, C. Electronic Properties of Oligoacenes from First Principles. *Phys. Rev. B* **2005**, *72* (20), 205205.

(25) Covarel, G.; Bensaid, B.; Boddaert, X.; Giljean, S.; Benaben, P.; Louis, P. Characterization of Organic Ultra-Thin Film Adhesion on Flexible Substrate Using Scratch Test Technique. *Surface and Coatings Technology* **2012**, *211*, 138–142.

(26) Tong, T.; Babatope, B.; Admassie, S.; Meng, J.; Akwogu, O.; Akande, W.; Soboyejo, W. O. Adhesion in Organic Electronic Structures. *Journal of Applied Physics* **2009**, *106* (8), 083708.

(27) Stewart, K. R.; Whitesides, G. M.; Godfried, H. P.; Silvera, I. F. Improved Adhesion of Thin Conformal Organic Films to Metal Surfaces. *Review of Scientific Instruments* **1986**, *57* (7), 1381–1383.

(28) Georgakopoulos, S.; Pérez-Rodríguez, A.; Campos, A.; Temiño, I.; Galindo, S.; Barrena, E.; Ocal, C.; Mas-Torrent, M. Spray-Coated Contacts from an Organic Charge Transfer Complex Solution for Organic Field-Effect Transistors. *Organic Electronics* **2017**, *48*, 365–370.

(29) Pfattner, R.; Rovira, C.; Mas-Torrent, M. Organic Metal Engineering for Enhanced Field-Effect Transistor Performance. *Phys. Chem. Chem. Phys.* **2015**, *17* (40), 26545–26552.

(30) Cho, J. H.; Kim, D. H.; Jang, Y.; Lee, W. H.; Ihm, K.; Han, J.-H.; Chung, S.; Cho, K. Effects of Metal Penetration into Organic Semiconductors on the Electrical Properties of Organic Thin Film Transistors. *Applied Physics Letters* **2006**, *89* (13), 132101.

(31) Watkins, N. J.; Yan, L.; Gao, Y. Electronic Structure Symmetry of Interfaces between Pentacene and Metals. *Applied Physics Letters* **2002**, *80* (23), 4384–4386.

(32) Hamadani, B. H.; Corley, D. A.; Ciszek, J. W.; Tour, J. M.; Natelson, D. Controlling Charge Injection in Organic Field-Effect Transistors Using Self-Assembled Monolayers. *Nano Letters* **2006**, *6* (6), 1303–1306.

(33) Campbell, I. H.; Kress, J. D.; Martin, R. L.; Smith, D. L.; Barashkov, N. N.; Ferraris, J. P. Controlling Charge Injection in Organic Electronic Devices Using Self-Assembled Monolayers. *Applied Physics Letters* **1997**, *71* (24), 3528–3530.

(34) Yang, H.; Yang, L.; Ling, M.-M.; Lastella, S.; Gandhi, D. D.; Ramanath, G.; Bao, Z.; Ryu, C. Y. Aging Susceptibility of Terrace-Like Pentacene Films. *The Journal of Physical Chemistry C* **2008**, *112* (42), 16161–16165.

(35) Vollmer, A.; Jurchescu, O. D.; Arfaoui, I.; Salzmann, I.; Palstra, T. T. M.; Rudolf, P.; Niemax, J.; Pflaum, J.; Rabe, J. P.; Koch, N. The Effect of Oxygen Exposure on Pentacene Electronic Structure. *The European Physical Journal E* **2005**, *17* (3), 339–343.

(36) Yoo, S. H.; Kum, J. M.; Cho, S. O. Tuning the Electronic Band Structure of PCBM by Electron Irradiation. *Nanoscale Research Letters* **2011**, *6* (1), 1–7.

(37) Calhoun, M. F.; Sanchez, J.; Olaya, D.; Gershenson, M. E.; Podzorov, V. Electronic Functionalization of the Surface of Organic Semiconductors with Self-Assembled

Monolayers. *Nat Mater* **2008**, *7* (1), 84–89.

(38) Storer, J. W.; Raimondi, L.; Houk, K. N. Theoretical Secondary Kinetic Isotope Effects and the Interpretation of Transition State Geometries. 2. The Diels-Alder Reaction Transition State Geometry. *Journal of the American Chemical Society* **1994**, *116* (21), 9675–9683.

(39) Piranej, S.; Turner, D. A.; Dalke, S. M.; Park, H.; Qualizza, B. A.; Vicente, J.; Chen, J.; Ciszek, J. W. Tunable Interfaces on Tetracene and Pentacene Thin-Films via Monolayers. *CrystEngComm* **2016**, *18* (32), 6062–6068.

(40) Brantley, S. L.; White, A. F.; Hodson, M. E. Surface Area of Primary Silicate Minerals. In *Growth, Dissolution and Pattern Formation in Geosystems*; Jamtveit, B., Meakin, P., Eds.; Springer Netherlands: Dordrecht, 1999; pp 291–326.

(41) Shaheen, A.; Sturm, J. M.; Ricciardi, R.; Huskens, J.; Lee, C. J.; Bijkerk, F. Characterization of Self-Assembled Monolayers on a Ruthenium Surface. *Langmuir* **2017**, *33* (25), 6419–6426.

(42) Paul, I. C.; Curtin, D. Y. Reactions of Organic Crystals with Gases. *Science* **1975**, *187*, 19–26.

(43) Paul, I. C.; Curtin, D. Y. Thermally Induced Organic Reactions in the Solid State. *Accounts of Chemical Research* **1973**, *6* (7), 217–225.

(44) Hamers, R. J. Flexible Electonics Futures. *Nature* **2001**, *412*, 489–490.

(45) Qualizza, B. A.; Ciszek, J. W. Experimental Survey of the Kinetics of Acene Diels–Alder Reactions. *Journal of Physical Organic Chemistry* **2015**, *28* (10), 629–634.

(46) Qualizza, B. A.; Prasad, S.; Chiarelli, M. P.; Ciszek, J. W. Functionalization of Organic Semiconductor Crystals via the Diels-Alder Reaction. *Chem. Commun.* **2013**, *49* (40), 4495–4497.

(47) Deye, G. J.; Vicente, J. R.; Dalke, S. M.; Piranej, S.; Chen, J.; Ciszek, J. W. The Role of Thermal Activation and Molecular Structure on the Reaction of Molecular Surfaces. *Langmuir* **2017**, *33* (33), 8140–8146.

(48) Boudinet, D.; Benwadih, M.; Altazin, S.; Verilhac, J.-M.; De Vito, E.; Serbutoviez, C.; Horowitz, G.; Facchetti, A. Influence of Substrate Surface Chemistry on the Performance of Top-Gate Organic Thin-Film Transistors. *Journal of the American Chemical Society* **2011**, *133* (26), 9968–9971.

(49) Guo, X.; Facchetti, A.; Marks, T. J. Imide- and Amide-Functionalized Polymer

Semiconductors. *Chemical Reviews* **2014**, *114* (18), 8943–9021.

(50) Hill, I. G.; Milliron, D.; Schwartz, J.; Kahn, A. Organic Semiconductor Interfaces: Electronic Structure and Transport Properties. *Applied Surface Science* **2000**, *166* (1–4), 354–362.

(51) Forrest, S. R. The Path to Ubiquitous and Low-Cost Organic Electronic Appliances on Plastic. *Nature* **2004**, *428* (6986), 911–918.

(52) Briseno, A. L.; Mannsfeld, S. C. B.; Ling, M. M.; Liu, S.; Tseng, R. J.; Reese, C.; Roberts, M. E.; Yang, Y.; Wudl, F.; Bao, Z. Patterning Organic Single-Crystal Transistor Arrays. *Nature* **2006**, *444* (7121), 913–917.

(53) Klauk, H.; Zschieschang, U.; Pflaum, J.; Halik, M. Ultralow-Power Organic Complementary Circuits. *Nature* **2007**, *445* (7129), 745–748.

(54) Tait, S. L.; Lim, H.; Theertham, A.; Seidel, P. First Layer Compression and Transition to Standing Second Layer of Terephthalic Acid on Cu(100). *Phys. Chem. Chem. Phys.* **2012**, *14* (22), 8217–8223.

(55) Fleming, I. *Pericyclic Reactions*; Oxford University Press: New York, 1999.

(56) Israelachvili, J. *Intermolecular and Surface Forces*, second.; Academic Press: London, 1991.

(57) Kaupp, G.; Schmeyers, J. Gas/Solid Reactions of Aliphatic Amines with Thiohydantoins: Atomic Force Microscopy and New Mechanisms. *Angewandte Chemie International Edition in English* **1993**, *32* (11), 1587–1589.

(58) Kaupp, G.; Schmeyers, J.; Boy, J. Quantitative Solid-State Reactions of Amines with Carbonyl Compounds and Isothiocyanates. *Tetrahedron* **2000**, *56* (36), 6899–6911.

(59) Setvín, M.; Aschauer, U.; Scheiber, P.; Li, Y.-F.; Hou, W.; Schmid, M.; Selloni, A.; Diebold, U. Reaction of O2 with Subsurface Oxygen Vacancies on TiO2 Anatase (101). *Science* **2013**, *341* (6149), 988–991.

(60) Wälchli, N.; Kampshoff, E.; Menck, A.; Kern, K. Silicide Growth at Metal Surfaces: Competition between Subsurface Diffusion and Chemical Reaction. *Surface Science* **1997**, *382* (1), L705–L712.

(61) Atwood, J. L.; Barbour, L. J.; Jerga, A.; Schottel, B. L. Guest Transport in a Nonporous Organic Solid via Dynamic van Der Waals Cooperativity. *Science* **2002**, *298* (5595), 1000–1002.

(62) Pensa, E.; Cortés, E.; Corthey, G.; Carro, P.; Vericat, C.; Fonticelli, M. H.; Benítez, G.; Rubert, A. A.; Salvarezza, R. C. The Chemistry of the Sulfur–Gold Interface: In Search of a Unified Model. *Accounts of Chemical Research* **2012**, *45* (8), 1183–1192.

(63) Campbell, R. B.; Robertson, J. M.; Trotter, J. The Crystal Structure of Hexacene, and a Revision of the Crystallographic Data for Tetracene. *Acta Crystallographica* **1962**, *15* (3), 289–290.

(64) Gharagheizi, F.; Sattari, M.; Tirandazi, B. Prediction of Crystal Lattice Energy Using Enthalpy of Sublimation: A Group Contribution-Based Model. *Industrial & Engineering Chemistry Research* **2011**, *50* (4), 2482–2486.

(65) Hoyer, H.; Peperle, W. Dampfdruckmessungen an Organischen Substanzen Und Ihre Sublimationswärmen. *Berichte der Bunsengesellschaft für physikalische Chemie* **1958**, *62*, 61–66.

(66) Nass, K.; Lenoir, D.; Kettrup, A. Calculation of the Thermodynamic Properties of Polycyclic Aromatic Hydrocarbons by an Incremental Procedure. *Angewandte Chemie International Edition in English* **1995**, *34* (16), 1735–1736.

(67) Nobuko, W.; Hiroo, I. Heats of Sublimation of Polycyclic Aromatic Hydrocarbons and Their Molecular Packings. *Bulletin of the Chemical Society of Japan* **1967**, *40* (10), 2267–2271.

(68) Marsh, R. E.; Ubell, E.; Wilcox, H. E. The Crystal Structure of Maleic Anhydride. *Acta Crystallographica* **1962**, *15* (1), 35–41.

(69) Hu, W. S.; Tao, Y. T.; Hsu, Y. J.; Wei, D. H.; Wu, Y. S. Molecular Orientation of Evaporated Pentacene Films on Gold: Alignment Effect of Self-Assembled Monolayer. *Langmuir* **2005**, *21* (6), 2260–2266.

(70) Morita, T.; Kimura, S.; Kobayashi, S.; Imanishi, Y. Photocurrent Generation under a Large Dipole Moment Formed by Self-Assembled Monolayers of Helical Peptides Having an N-Ethylcarbazolyl Group. *Journal of the American Chemical Society* **2000**, *122* (12), 2850–2859.

(71) Ye, R.; Baba, M.; Suzuki, K.; Ohishi, Y.; Mori, K. Effect of Thermal Annealing on Morphology of Pentacene Thin Films. *Japanese Journal of Applied Physics* **2003**, *42* (7R), 4473.

(72) English, C. R.; Bishop, L. M.; Chen, J.; Hamers, R. J. Formation of Self-Assembled Monolayers of π-Conjugated Molecules on TiO2 Surfaces by Thermal Grafting of Aryl and Benzyl Halides. *Langmuir* **2012**, *28* (17), 6866–6876.

(73) Kiselev, V. D.; Konovalov, A. I. Internal and External Factors Influencing the Diels–Alder Reaction. *Journal of Physical Organic Chemistry* **2009**, *22* (5), 466–483.

(74) Schleyer, P. von R.; Manoharan, M.; Jiao, H.; Stahl, F. The Acenes: Is There a Relationship between Aromatic Stabilization and Reactivity? *Organic Letters* **2001**, *3* (23), 3643–3646.

(75) Filler, M. A.; Bent, S. F. The Surface as Molecular Reagent: Organic Chemistry at the Semiconductor Interface. *Progress in Surface Science* **2003**, *73* (1–3), 1–56.

(76) Lide, D. R. *CRC Handbook of Chemistry and Physics, 83rd Edition*, 83rd ed.; CRC Press, 2002.

(77) Ma, H.; Yip, H.-L.; Huang, F.; Jen, A. K.-Y. Interface Engineering for Organic Electronics. *Advanced Functional Materials* **2010**, *20* (9), 1371–1388.

(78) Dennes, T. J.; Schwartz, J. A Nanoscale Metal Alkoxide/Oxide Adhesion Layer Enables Spatially Controlled Metallization of Polymer Surfaces. *ACS Appl. Mater. Interfaces* **2009**, *1* (10), 2119–2122.

(79) Braun, S.; Salaneck, W. R.; Fahlman, M. Energy-Level Alignment at Organic/Metal and Organic/Organic Interfaces. *Advanced Materials* **2009**, *21* (14–15), 1450–1472.

(80) Bikondoa, O.; Pang, C. L.; Ithnin, R.; Muryn, C. A.; Onishi, H.; Thornton, G. Direct Visualization of Defect-Mediated Dissociation of Water on TiO2(110). *Nature Materials* **2006**, *5*, 189.

(81) Henrich, V. E.; Cox, P. A. *The Surface Science of Metal Oxides*; Cambridge University Press: University Press, Cambridge, 1994.

(82) Nickel, B.; Barabash, R.; Ruiz, R.; Koch, N.; Kahn, A.; Feldman, L. C.; Haglund, R. F.; Scoles, G. Dislocation Arrangements in Pentacene Thin Films. *Phys. Rev. B* **2004**, *70* (12), 125401.

(83) McCullough, J. D.; Curtin, D. Y.; Paul, I. C. Beckmann-Chapman Rearrangement in the Solid State of Oxime Picryl Ethers. *Journal of the American Chemical Society* **1972**, *94* (3), 874–882.

(84) Cohen, M. D.; Ludmer, Z.; Thomas, J. M.; Williams, J. O. The Role of Structural Imperfections in the Photodimerization of 9-Cyanoanthracene. *Proc R Soc Lond A Math Phys Sci* **1971**, *324* (1559), 459.

(85) Laudise, R. A.; Kloc, C.; Simpkins, P. G.; Siegrist, T. Physical Vapor Growth of Organic Semiconductors. *Journal of Crystal Growth* **1998**, *187* (3), 449–454.

(86) Seo, S.; Grabow, L. C.; Mavrikakis, M.; Hamers, R. J.; Thompson, N. J.; Evans, P. G. Molecular-Scale Structural Distortion near Vacancies in Pentacene. *Applied Physics Letters* **2008**, *92* (15), 153313.

(87) Verlaak, S.; Rolin, C.; Heremans, P. Microscopic Description of Elementary Growth Processes and Classification of Structural Defects in Pentacene Thin Films. *The Journal of Physical Chemistry B* **2007**, *111* (1), 139–150.

(88) Seo, S.; Evans, P. G. Molecular Structure of Extended Defects in Monolayer-Scale Pentacene Thin Films. *Journal of Applied Physics* **2009**, *106* (10), 103521.

(89) Lee, H. S.; Kim, D. H.; Cho, J. H.; Hwang, M.; Jang, Y.; Cho, K. Effect of the Phase States of Self-Assembled Monolayers on Pentacene Growth and Thin-Film Transistor Characteristics. *Journal of the American Chemical Society* **2008**, *130* (32), 10556–10564.

(90) Bock, C.; Pham, D. V.; Kunze, U.; Käfer, D.; Witte, G.; Wöll, C. Improved Morphology and Charge Carrier Injection in Pentacene Field-Effect Transistors with Thiol-Treated Electrodes. *Journal of Applied Physics* **2006**, *100* (11), 114517.

(91) Kim, D. H.; Lee, H. S.; Yang, H.; Yang, L.; Cho, K. Tunable Crystal Nanostructures of Pentacene Thin Films on Gate Dielectrics Possessing Surface-Order Control. *Advanced Functional Materials* **2008**, *18* (9), 1363–1370.

(92) Celle, C.; Suspène, C.; Ternisien, M.; Lenfant, S.; Guérin, D.; Smaali, K.; Lmimouni, K.; Simonato, J. P.; Vuillaume, D. Interface Dipole: Effects on Threshold Voltage and Mobility for Both Amorphous and Poly-Crystalline Organic Field Effect Transistors. *Organic Electronics* **2014**, *15* (3), 729–737.

(93) Hill, I. G.; Weinert, C. M.; Kreplak, L.; van Zyl, B. P. Influence of Self-Assembled Monolayer Chain Length on Modified Gate Dielectric Pentacene Thin-Film Transistors. *Applied Physics A* **2009**, *95* (1), 81–87.

(94) Fukuda, K.; Hamamoto, T.; Yokota, T.; Sekitani, T.; Zschieschang, U.; Klauk, H.; Someya, T. Effects of the Alkyl Chain Length in Phosphonic Acid Self-Assembled Monolayer Gate Dielectrics on the Performance and Stability of Low-Voltage Organic Thin-Film Transistors. *Applied Physics Letters* **2009**, *95* (20), 203301.

(95) Acton, B. O.; Ting, G. G.; Shamberger, P. J.; Ohuchi, F. S.; Ma, H.; Jen, A. K.-Y. Dielectric Surface-Controlled Low-Voltage Organic Transistors via n-Alkyl Phosphonic Acid Self-Assembled Monolayers on High-k Metal Oxide. *ACS Applied Materials & Interfaces* **2010**, *2* (2), 511–520.

(96) Lang, P.; Mottaghi, D.; Lacaze, P.-C. On the Relationship between the Structure of Self-Assembled Carboxylic Acid Monolayers on Alumina and the Organization and Electrical

Properties of a Pentacene Thin Film. *Applied Surface Science* **2016**, *365* (Supplement C), 364–375.

(97) Pratontep, S.; Brinkmann, M.; Nüesch, F.; Zuppiroli, L. Nucleation and Growth of Ultrathin Pentacene Films on Silicon Dioxide: Effect of Deposition Rate and Substrate Temperature. *Synthetic Metals* **2004**, *146* (3), 387–391.

(98) Venables, J. A.; Spiller, G. D. T.; Hanbucken, M. Nucleation and Growth of Thin Films. *Reports on Progress in Physics* **1984**, *47* (4), 399.

(99) Stadlober, B.; Haas, U.; Maresch, H.; Haase, A. Growth Model of Pentacene on Inorganic and Organic Dielectrics Based on Scaling and Rate-Equation Theory. *Phys. Rev. B* **2006**, *74* (16), 165302.

(100) Kalihari, V.; Tadmor, E. B.; Haugstad, G.; Frisbie, C. D. Grain Orientation Mapping of Polycrystalline Organic Semiconductor Films by Transverse Shear Microscopy. *Advanced Materials* **2008**, *20* (21), 4033–4039.

(101) Minakata, T.; Imai, H.; Ozaki, M.; Saco, K. Structural Studies on Highly Ordered and Highly Conductive Thin Films of Pentacene. *Journal of Applied Physics* **1992**, *72* (11), 5220–5225.

(102) Porter, M. D.; Bright, T. B.; Allara, D. L.; Chidsey, C. E. D. Spontaneously Organized Molecular Assemblies. 4. Structural Characterization of n-Alkyl Thiol Monolayers on Gold by Optical Ellipsometry, Infrared Spectroscopy, and Electrochemistry. *Journal of the American Chemical Society* **1987**, *109* (12), 3559–3568.

(103) Laibinis, P. E.; Whitesides, G. M.; Allara, D. L.; Tao, Y. T.; Parikh, A. N.; Nuzzo, R. G. Comparison of the Structures and Wetting Properties of Self-Assembled Monolayers of n-Alkanethiols on the Coinage Metal Surfaces, Copper, Silver, and Gold. *Journal of the American Chemical Society* **1991**, *113* (19), 7152–7167.

(104) Griffiths, P. R.; de Haseth, J. A. *Fourier Transform Infrared Spectrometry*, 2nd ed.; John Wiley & Sons, 2007.

# VITA

Gregory J. Deye is from Palos Park, Illinois. In 2013, he earned a Bachelor of Science in chemistry with a minor in physics from Marquette University. From 2013 to 2014, Gregory took graduate level chemistry courses and performed research at the Illinois Institute of Technology. As his interests in surface chemistry and organic electronics developed, Gregory relocated to Loyola University Chicago to pursue a Ph.D. in chemistry under the direction of Professor Jacob W. Ciszek. Since then, Gregory has worked on several projects concerning surface reactions on organic semiconductors. Of note, Gregory published a paper in the high impact journal, Langmuir, and another paper is forthcoming concerning content in chapter 3. During his tenure at Loyola University Chicago, Gregory also presented at numerous conferences including the Materials Research Society Spring Meeting and AVS Prairie Chapter. Following graduation, Gregory will pursue an industry-based surface chemistry career in Phoenix, AZ.